



CZECH TECHNICAL UNIVERSITY IN PRAGUE  
Faculty of Civil Engineering  
Department of Mechanics

---

# **Vícekriteriální optimalizace léčebného plánu protonové terapie**

## **Multi-criteria optimization of proton therapy treatment plan**

Bachelor thesis

Study program:	Civil Engineering
Branch of Study:	Building Structures
Thesis supervisor:	Doc. Ing. Matěj Lepš, Ph.D.

**Marek Tyburec**

---

Prague 2015



## ZADÁNÍ BAKALÁŘSKÉ PRÁCE

studijní program: Stavební inženýrství

studijní obor: Konstrukce pozemních staveb

akademický rok: 2014/2015

Jméno a příjmení studenta: Marek Tyburec

Zadávací katedra: Katedra mechaniky

Vedoucí bakalářské práce: doc. Ing. Matěj Lepš, Ph.D.

Název bakalářské práce: Vícekritériální optimalizace léčebného plánu protonové terapie

Název bakalářské práce  
v anglickém jazyce: Multi-criteria optimization of proton therapy treatment plan

Rámcový obsah bakalářské práce: Rešerše dostupné literatury; implementace Braggovy křivky  
v 1D, v rovině a v prostoru; porovnání aproximace s existující literaturou;  
zahrnutí nehomogenit do aproximace; formulace úlohy lineárního programování;  
grafické zobrazení léčebného plánu; implementace vícekritériální optimalizace;  
paralelizace výpočtů; zpracování a prezentace výsledků

Datum zadání bakalářské práce: 3.2.2015


Termín odevzdání:

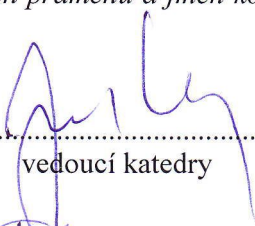
**15.5.2015**

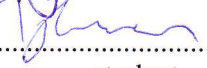
(vyplňte poslední den výuky  
příslušného semestru)

Pokud student neodevzdal bakalářskou práci v určeném termínu, tuto skutečnost předem písemně zdůvodnil a omluva byla děkanem uznána, stanoví děkan studentovi náhradní termín odevzdání bakalářské práce. Pokud se však student řádně neomluvil nebo omluva nebyla děkanem uznána, může si student zapsat bakalářskou práci podruhé. Studentovi, který při opakovaném zápisu bakalářskou práci neodevzdal v určeném termínu a tuto skutečnost řádně neomluvil nebo omluva nebyla děkanem uznána, se ukončuje studium podle § 56 zákona o VŠ č. 111/1998. (SZŘ ČVUT čl. 21, odst. 4)

*Student bere na vědomí, že je povinen vypracovat bakalářskou práci samostatně, bez cizí pomoci, s výjimkou poskytnutých konzultací. Seznam použité literatury, jiných pramenů a jmen konzultantů je třeba uvést v bakalářské práci.*

  
.....  
vedoucí bakalářské práce

  
.....  
vedoucí katedry

  
.....  
student

Zadání bakalářské práce převzal dne: 3.2.2015

Formulář nutno vyhotovit ve 3 výtiscích – 1x katedra, 1x student, 1x studijní odd. (zašle katedra)

Nejpozději do konce 2. týdne výuky v semestru odešle katedra 1 kopii zadání BP na studijní oddělení a provede zápis údajů týkajících se BP do databáze KOS.

BP zadává katedra nejpozději 1. týden semestru, v němž má student BP zapsanou.

(Směrnice děkana pro realizaci studijních programů a SZZ na FSv ČVUT čl. 5, odst. 7)

# Statutory declaration

I declare that I have developed and written the enclosed bachelor thesis "Multi-criteria optimization of proton therapy treatment" completely by myself just under professional supervision of doc. Ing. Matěj Lepš, Ph.D.

I also declare that all used literature is listed in References.

Date: .....

Signature: .....

# Acknowledgement

I would like to express my sincere gratitude to doc. Ing. Matěj Lepš, Ph.D. because of his professional supervision, valuable suggestions and helpful feedback.

This thesis has been realized with the financial support of A Foundation Supporting High-tech R&D, Innovations and Technical Education in the Czech Republic – ČVUT Media Lab.

# Abstrakt

Tato práce se zabývá vícekritériální optimalizací léčebného plánu protonové terapie.

Nejprve je představen zjednodušený model šíření záření prostorem, tj. je zavedena Bortfeldova analytická aproximace popisu šíření protonů v homogenním médiu, je zaveden vliv změny prostředí a nehomogenit. Vliv změny směru záření – mnohonásobný rozptyl – je zaveden Highlandovou aproximací.

V následující části práce je ve stručnosti představeno vícekritériální lineární programování a několik možných přístupů vedoucích k jeho řešení, zejména Bensonův algoritmus, resp. jeho paralelní a ne-paralelní verze.

Samotná optimalizace je nejprve definována jako lineární program, ve kterém se minimalizuje množství vyzářených protonů. Z důvodu řešitelnosti je problém upraven na lineární program s volnými cíli. Finální modifikací je vícekritériální řešení lineárního programu s volnými cíli, které umožní výběr nejvhodnějšího řešení rozhodovatelem.

V závěru práce je vyhodnocena časová náročnost implementace popsané v této práci a jsou shrnuty její výhody.

# Abstract

This thesis deals with multi-criteria optimization of proton therapy treatment plan.

Firstly, an approximate model describing radiation spread in a space is introduced: Bortfeld's analytical approximation of the Bragg curve in homogeneous media and the influence of inhomogeneities. Direction change of a proton beam is implemented using generalized Highland's approximation of the theory of multiple scattering.

In the second chapter we shortly present some approaches leading towards the solution of multiple-objective linear programming (MOLP), especially parallel and non-parallel versions of Benson's algorithm and a developed approach to an approximate Pareto surface based on a uniform distribution.

The optimization of the treatment plan is firstly defined as a linear program minimizing the amount of irradiated protons. Due to the uncertainty of feasibility of the formulation a linear program with free goals is introduced. Finally, we enhance the formulation to a multi-objective linear program with free goals, enabling thus the decision maker to choose the most appropriate treatment plan suitable for the particular patient.

In the conclusion time demands of the implementation are evaluated.

# Klíčová slova

Rešerše dostupné literatury; implementace Braggovy křivky v 1D, v rovině a v prostoru; porovnání aproximace s existující literaturou; zahrnutí nehomogenit do aproximace; formulace úlohy lineárního programování; grafické zobrazení léčebného plánu; implementace vícekriteriální optimalizace; paralelizace výpočtů; zpracování a prezentace výsledků.

# Keywords

Review of state-of-the-art; implementation of Bragg curve in 1D, plane and in space; comparison of approximation with current literature; evaluating inhomogeneities; formulation of a linear program; graphical display of multi-objective treatment plan; parallelization; evaluation and presentation of results.

# Contents

<b>1</b>	<b>Introduction</b>	<b>1</b>
1.1	Radiotherapy . . . . .	1
1.2	Comparison of proton and photon therapy . . . . .	2
1.3	Proton therapy treatment plan . . . . .	3
<b>2</b>	<b>Beam propagation through matter</b>	<b>4</b>
2.1	Analytical approximation of the Bragg curve . . . . .	4
2.2	Influence of inhomogeneities on the Bragg curve . . . . .	7
2.3	Multiple scattering theory . . . . .	10
<b>3</b>	<b>Multi-objective programming</b>	<b>13</b>
3.1	Formulation of multi-objective programming . . . . .	13
3.1.1	Dominated and non-dominated solution . . . . .	13
3.1.2	Pareto set and Pareto surface . . . . .	14
3.2	Multi-objective linear programming . . . . .	14
3.2.1	Aggregation of objective functions . . . . .	15
3.2.2	Compromise solution according to the maximal component . . . . .	16
3.2.3	Minimization of the distance from ideal values . . . . .	18
3.2.4	Goal programming . . . . .	18
3.2.5	Benson's algorithm . . . . .	20
3.2.6	Non-dominated solutions uniformly distributed on the Pareto surface . . . . .	24
<b>4</b>	<b>Optimization of proton therapy treatment plan</b>	<b>27</b>
4.1	Formulation of the optimization problem . . . . .	27
4.1.1	Objective function . . . . .	27
4.1.2	Linear program formulation . . . . .	28
4.2	Selection of an appropriate solution . . . . .	29
4.3	Examples of optimization . . . . .	30
4.3.1	Minimization of primary fluences . . . . .	30
4.3.2	Linear goal programming . . . . .	33
4.3.3	Multi-objective linear goal programming . . . . .	34
4.4	Time demands of the optimization using Benson's algorithm . . . . .	40



<i>CONTENTS</i>	viii
<b>5 Conclusion</b>	<b>41</b>
<b>Appendix</b>	<b>I</b>
<b>A Modified algorithm distmesh</b>	<b>I</b>
<b>B Numerical solution of definite integrals</b>	<b>III</b>

# List of Tables

2.1	Accuracy in the computation of WET . . . . .	10
2.2	Comparison of accuracy in computation of the characteristic multiple scattering angle. . . . .	12
4.1	1D example of one-sided irradiation. Dose is computed only in depths, where the constraints are checked. . . . .	30
4.2	Vertices of the polytope. . . . .	32
4.3	Time demands of the treatment plan optimization using Benson's algorithm. . . . .	40

# List of Figures

1.1	Comparison of absorbed dose of protons and photons in water. . . . .	2
1.2	Comparison of IMRT and IMPT treatment plan. . . . .	3
2.1	Elementary parameters of the Bragg curve shown on the proton beam accelerated to the initial kinetic energy $E_0 = 158.6$ MeV. . . . .	4
2.2	Influence of the initial kinetic energy $E_0$ on the dose in water. . . . .	5
2.3	Influence of the initial kinetic energy $E_0$ on the proportional dose in water. . . . .	5
2.4	Dependence of $R_0 - z_{\max}$ on the initial energy $E_0$ in water medium. . . . .	7
2.5	Influence of inhomogeneities on the shape of Bragg curve. . . . .	8
2.6	The dependence of the multiple scattering angle $\theta$ on the depth $z$ and on $y$ . . . . .	11
3.1	Convex and non-convex Pareto surface. . . . .	14
3.2	Example – aggregation of objective functions. . . . .	16
3.3	Example – compromise solution according to maximal component . . . . .	17
3.4	Compromise solution according to maximal component – dominated solution. . . . .	17
3.5	Example – minimization of the distance from ideal values . . . . .	19
3.6	Example – goal programming . . . . .	20
3.7	Example – Benson’s algorithm . . . . .	23
3.8	Example – Pareto-optimal solutions distributed uniformly on Pareto surface. . . . .	25
4.1	Free one-sided goals in optimization of proton therapy treatment plan. . . . .	29
4.2	Constraints in the 1D proton therapy treatment plan optimization. . . . .	31
4.3	Globally optimal solution of a simple 1D treatment plan. . . . .	32
4.4	Globally optimal solution of a simple 1D treatment plan – DVH of the tumor. . . . .	32
4.5	Optimal 1D treatment plan accounting the effect of inhomogeneities and double-sided irradiation. . . . .	33
4.6	Optimal 1D treatment plan optimized using linear goal programming. Double-sided irradiation. . . . .	34
4.7	Implementation of the user interface for displaying results of 1D multi-objective linear goal program. . . . .	35
4.8	Implementation of the user interface for displaying the results of linear goal program – Pareto surface. . . . .	36

4.9	Implementation of the user interface for displaying results of the multi-objective linear goal program for the 3D treatment plan. The cut at plane $x = 9.75$ cm is displayed. . . . .	37
4.10	Implementation of the user interface for displaying results of the multi-objective linear goal program for 3D treatment plan – 2D Pareto surface. . . . .	38
4.11	3D treatment plan accounting double-sided irradiation. The non-dominated solution shown in the figure conserves the required dose $D_{\text{TAR,min}}$ . . . . .	39
4.12	3D treatment plan accounting double-sided irradiation. The non-dominated solution shown in the figure conserves the required dose $D_{\text{OAR,max}}$ . . . . .	39
A.1	Example 2D problem solved by the modified algorithm <code>distmesh</code> . . . . .	II

# Chapter 1

## Introduction

Oncologic diseases are one of the most frequent<sup>1</sup> causes of death not only in the Czech Republic<sup>2</sup>. Depending on the diagnosis the treatment of patients can be divided into chemotherapy, surgery and radiotherapy. Radiotherapy is based on irradiation of a malignant tumor by ionizing radiation while minimizing consequences for the surrounding healthy tissues. The most commonly used particles are electrons and photons, however recently hadrons, i.e. protons and light ions, have gained in importance.

## Radiotherapy

Based on the location of the source of irradiation it is possible to divide radiotherapy into external beam radiotherapy and brachytherapy. In brachytherapy the radiation source, either liquid or solid, gets close to irradiated tumor, hence only little damaging the surrounding healthy tissue. In external beam radiotherapy the radiation source is, on the contrary, placed outside of the patient's body. Because radiation spreads towards the tumor through skin and other tissues it is meant to be less sparing (Hynková, Doleželová, Šlampa).

To destroy the tumor, also referred to as the target TAR, a determinate minimal dose is prescribed by a doctor. As the dose value is high the patient needs to be irradiated multiple times by a lower dose to avoid side effects. The same way a particular maximal dose for surrounding Organs at Risk (OARs) and eventually for all the surrounding (normal) tissues is defined to prevent their damage.

Particle streams passing through tissues cause their ionization, excitation of molecules and the formation of free radicals, consequently damaging DNA of the individual cells. After irradiation the cells use DNA repair mechanism. The ability of tumor cells to repair DNA is, however, lower, hence if the dose quantity is sufficient the tumor cells are either destroyed or prevented to divide.

To create the treatment plan it is firstly needed to assess a three-dimensional model of tissues surrounding tumor, for which magnetic resonance imaging (MRI) or computed tomography (CT) are used. The output of MRI and CT are two-dimensional slices with 0.46875 mm or 0.9375 mm precision

---

<sup>1</sup>According to (sta, 2013) cancer is the 2<sup>nd</sup> most frequent cause of death in the Czech Republic; most frequently the Czechs die because of the failure of the circulatory system.

<sup>2</sup>According to the statistics of World Cancer Research Fund (WCRF) there are annually indicated 293.8 patients with cancer on 100000 inhabitants, which leads to 14<sup>th</sup> most frequent incidence in the world (Wcrf.org, 2015).

in 3 mm or 5 mm distances. From the slices it is then possible to build the complete 3D model (Schlegel et al., 2006).

The spacial grid is then deployed by individual beams; and their intensities, i.e. primary fluencies, are optimized. The aim of the optimization procedure is to fulfill the required minimal dose in tumor and not to exceed the maximal dose in OARs. The optimization of individual beam intensities is usually referred to as Intensity Modulated Radiation Therapy (IMRT) or in the case of protons as Intensity Modulated Proton Therapy (IMPT). By the usage of individual intensities optimization it is also possible to irradiate complex geometries.

In the preparation of the treatment plan for IMPT or IMRT, so called inverse planning is used. Firstly, a doctor specifies tumor and OARs and assigns related dose limits. All the anatomically important structures mentioned above are drawn as a contours into CT or MRI slices. Finally an optimization program computes primary fluencies to fulfill the prescribed assignment (Hynková, Doleželová, Šlampa).

## Comparison of proton and photon therapy

In both proton and photon therapy the particles are accelerated in a circular particle accelerator (either cyclotron or synchrotron) to the required kinetic energy. Note that in the proton therapy the energy range is usually between 70-230 MeV. The dose irradiated in the direction  $z$  is dependent also on used particles. For comparison, the dose valid for protons and photons spreading through water environment is shown in Figure 1.1.

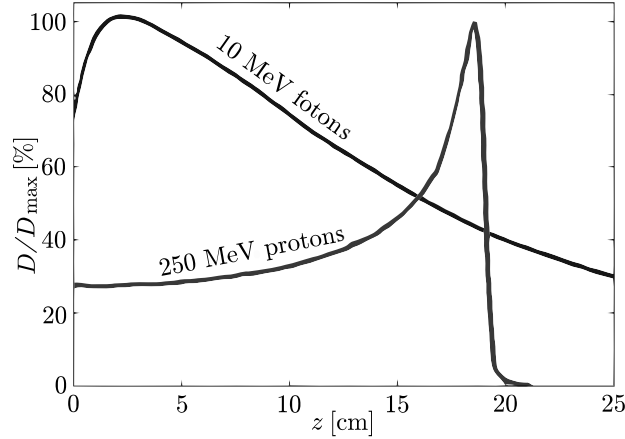


Figure 1.1: Comparison of absorbed dose of protons and photons in water as a function of the depth  $z$ . Proton beam takes a significant extreme point – Bragg peak. The figure has been copied from (Lang, Riesterer, 2013).

In the case of protons the largest amount of dose is absorbed by water in a short interval called the Bragg peak. The distance of the Bragg peak from the source of radiation is dependent on the kinetic energy of protons, hence it is possible to achieve sufficient irradiation of tumor and concurrently to save the healthy tissues and avoid the OARs. For photons the largest amount of dose is absorbed in a small distance from the radiation source, usually ahead of the tumor. The amount of absorbed dose

gradually decreases and therefore the tissues behind the tumor are also affected. Due to the lower absorbed dose in healthy tissues the more expensive proton therapy is used mainly for tumors close to OARs – brain, eyes, neck, prostate etc., see Figure 1.2 for a reference example.

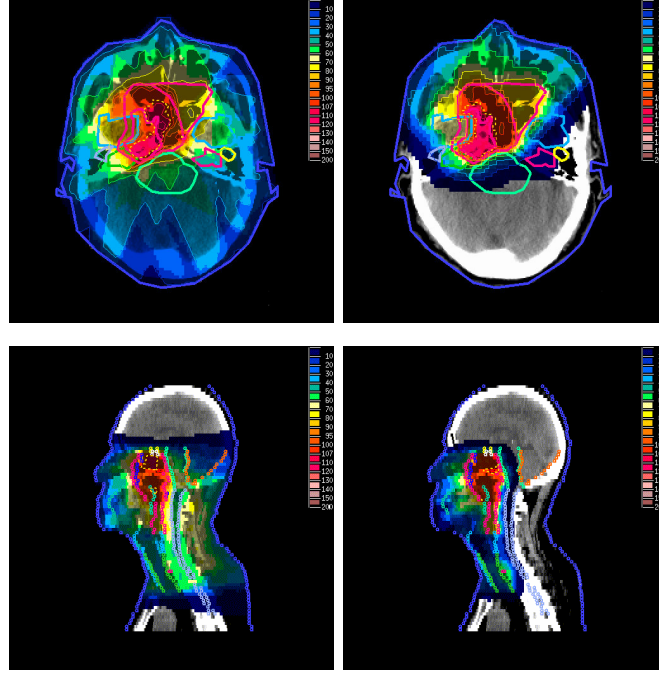


Figure 1.2: Comparison of IMRT (left) and IMPT (right) treatment plan. The figure has been copied from (Taheri-Kadkhoda et al., 2008).

## Proton therapy treatment plan

Individual proton beams are computed by a very accurate but also time demanding probabilistic Monte Carlo method. The subsequent optimization can then last even half a day. The optimal treatment plans are thus prepared in advance, after the patient's last visit before irradiation. Due to the daily dose limits the patient is usually irradiated multiple times with the interval of several days.

In the resulting time spaces the tumor can change its shape, even very drastically, and the prepared treatment plan then does not make any sense. It is therefore needed to create a new one as soon as possible to reflect the changes.

This thesis deals with a simplified model of a beam propagation through matter and introduces the influence of inhomogeneities. The spacial effect of the beam caused by multiple scattering is also considered. This thesis further introduces multi-objective linear programming (MOLP) and establishes a multi-objective model to acquire whole Pareto Surface (PS) of a given MOLP. Also a developed algorithm for an approximation of the whole Pareto surface is presented. The theory is then applied on the multi-objective optimization of proton therapy treatment plan.

The aim of this thesis is to assemble and solve the optimization problem in MATLAB software, reducing the computational time as much as possible to enable the doctors to reflect changes in the geometry of tumor and its surroundings.

## Chapter 2

# Beam propagation through matter

Cancer treatment using radiotherapy is based on the principle of destroying the tumor by a certain dose. It is therefore crucial to determine the dependence between the absorbed dose and distance of the source of irradiation. In proton therapy this dependence is stated by a Bragg curve.

### Analytical approximation of the Bragg curve

In the year of 1997 Thomas Bortfeld derived an analytical approximation of the Bragg curve for proton beams (Bortfeld, 1997). The Bragg curve has been stated as a function of the initial kinetic energy<sup>1</sup>  $E_0$  that has been given to the particles in accelerator. In the consequence of collisions of protons with ambient particles the energy of protons gradually decreases up to the distance  $R_0$ , called range, where the energy of exactly one half of protons, originally accelerated to  $E_0$ , is equal to zero. The physical meaning of the range  $R_0$  is shown in Figure 2.1.

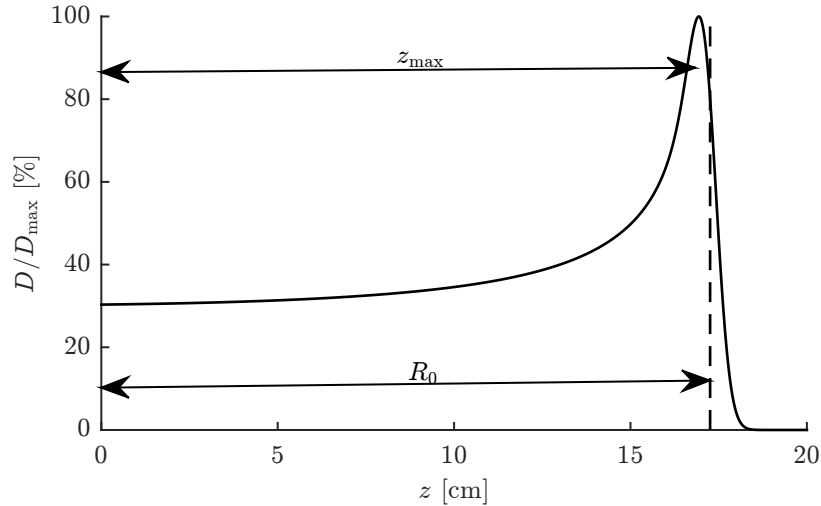


Figure 2.1: Elementary parameters of the Bragg curve shown on the proton beam accelerated to the initial kinetic energy  $E_0 = 158.6$  MeV.

The relation between the range and the initial kinetic energy can be found in tables, see e.g. (Janni, 1982) or (Berger et al., 1993); or it can be approximated the Bragg-Kleemann rule:

<sup>1</sup>The physical unit of energy in quantum mechanics is MeV.



$$R_0 \approx \alpha E_0^p, \quad (2.1)$$

where the proportionality factor  $\alpha$  and the exponent of energy-range relation  $p$  are material properties matching the experimentally measured values. The Equation (2.1) implies that the higher the initial kinetic energy  $E_0$ , the higher the range  $R_0$  of the Bragg curve and the more distant the depth  $z_{\max}$  of the Bragg peak. The impact of the initial energy on the range is shown in Figure 2.2. From Figure 2.3 it follows that the greatest ratio of the dose in the Bragg peak to the 'tail' dose happens when the range is short. Therefore, to save the healthy tissues surrounding the tumor the shortest path of the beam is usually advantageous.

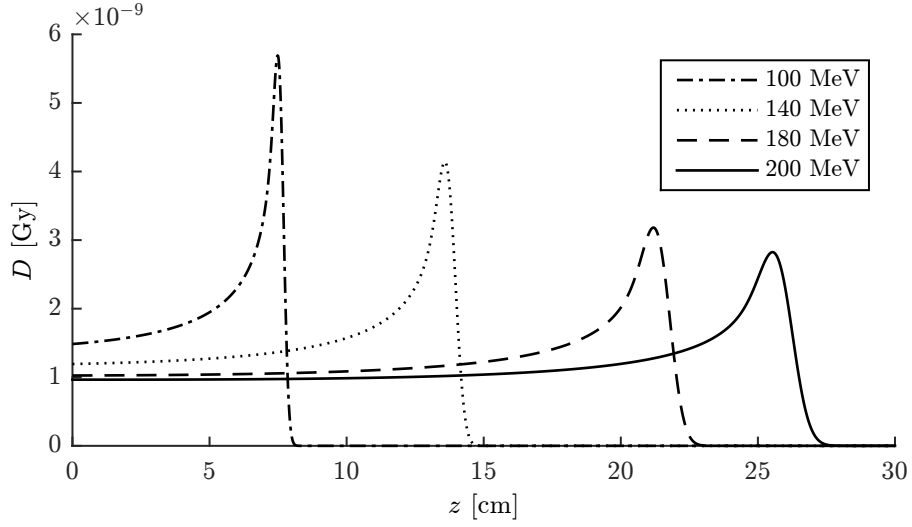


Figure 2.2: Influence of the initial kinetic energy  $E_0$  on the dose in water.

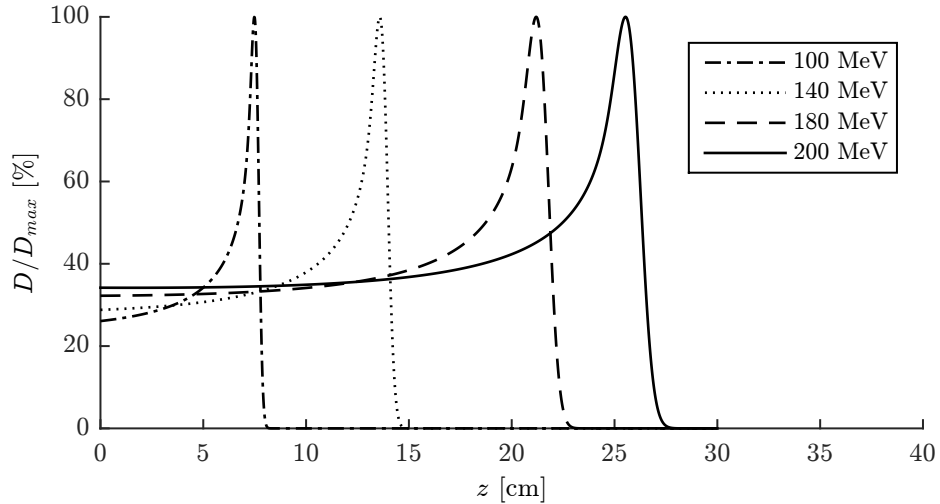


Figure 2.3: Influence of the initial kinetic energy  $E_0$  on the proportional dose in water.

We have already outlined that the range  $R_0$  of the proton beam is evaluated statistically, because the range of individual protons differs and collisions of individual protons are random. Therefore, even protons with equal initial kinetic energy  $E_0$  do not deliver the equal dose in the same depth  $z$ . Bortfeld (Bortfeld, 1997) thus established a Gaussian spectrum  $\sigma$  evaluating the range straggling and

the uncertainty of the kinetic initial energy of protons:

$$\sigma = \sqrt{\left(\alpha' \frac{p^3 \alpha^{2/p}}{3p-2} R_0^{3-2p}\right)^2 + (0.01 E_0)^2 \alpha^2 p^2 E_0^{2p-2}}, \quad (2.2)$$

where the constant  $\alpha'$  is a material property dependent on electron density (Bortfeld, 1997).

The resulting Bragg curve<sup>2</sup>  $D$  is the sum of all Gaussian distributions along the depth  $z$ . The resulting equation is thus

$$D(z, E_0) = \Phi_0 \frac{e^{-\frac{\zeta(z, E_0)^2}{4}} \sigma(E_0)^{1/p} \Gamma(1/p)}{\sqrt{2\pi} \rho \alpha^{1/p} [1 + \beta(R_0(E_0))]} \times \\ \times \left[ \frac{1}{\sigma(E_0)} \mathcal{P}_{-1/p}(-\zeta(z, E_0)) + \left( \frac{\beta}{p} + \gamma\beta + \frac{\epsilon}{R_0(E_0)} \right) \mathcal{P}_{-1/p-1}(-\zeta(z, E_0)) \right]. \quad (2.3)$$

In Equation (2.3) there appear several types of variables. The first are material properties: in addition to the already defined  $\alpha$  and  $p$ , the material density  $\rho$  also belong to this variable group as well as the fraction of primary fluence contributing to the 'tail' of the energy spectrum  $\epsilon$ , the slope parameter of the fluence reduction relation  $\beta$  and the fraction of locally absorbed energy released in nonelastic nuclear interactions  $\gamma$ . Specific values valid for water medium has been taken from (Bortfeld, 1997). The above equation then includes variables dependent on the initial kinetic energy  $E_0$ , specifically the Gaussian spectrum  $\sigma$  and also  $\zeta$  defined by the equation

$$\zeta(z, E_0) = \frac{R_0(E_0) - z}{\sigma}, \quad (2.4)$$

where the symbol  $\mathcal{P}$  denotes parabolic cylinder function (Weisstein, 2005). The shape of the resulting Bragg curve is shown in Figure 2.1.

For the optimization of treatment plan the most important variable is the primary fluence<sup>3</sup>  $\Phi_0$ . Fluence denotes the number of quantities of the radiation passing in one second through a unit surface orthogonal to the direction of propagation of the quantities. The primary fluence is thus bounded to the depth  $z = 0$  cm. It should be noted that the dose  $D(z)$  is linearly dependent on the primary fluence.

When assembling the treatment plan it is appropriate to place individual Bragg curves based on the position of the peak  $z_{\max}$ . We have thus approximated the relation between the initial energy  $E_0$  and the position of the peak, see Figure 2.4. The Bragg curves have been evaluated with a sufficient precision of 0.1 mm in the range of 1 MeV up to 300 MeV, including thus all the energies commonly used in proton therapy (Paganetti, 2012). The location of the Bragg peak, i.e. the variable  $z_{\max}$  has thus been evaluated with the precision of 0.1 mm.

Let us now begin with Equation (2.1) and the approximated relation given by a 4<sup>th</sup> level polynomial. We can then write

$$R_0 - z = a_1 E_0^4 + a_2 E_0^3 + a_3 E_0^2 + a_4 E_0 + a_5, \quad (2.5)$$

where  $a_1$  through  $a_5$  are material constants. The equation is subsequently rewritten to

<sup>2</sup>The physical unit of dose is a Gray (Gy). One Gray corresponds to the absorption of 1 J of energy in 1 kg of the material.

<sup>3</sup>The physical unit of fluence is (number of particles/s)/m<sup>2</sup>

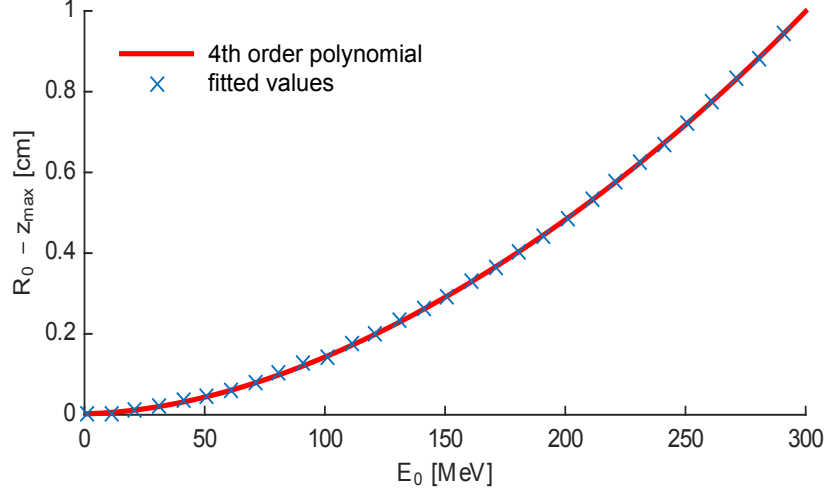


Figure 2.4: Dependence of  $R_0 - z_{\max}$  on the initial energy  $E_0$  in water medium.

$$z_{\max} = \alpha E_0^p - a_1 E_0^4 - a_2 E_0^3 - a_3 E_0^2 - a_4 E_0 - a_5. \quad (2.6)$$

Comparing the hereby computed values of the Bragg peak with the values evaluated within the precision of 0.1 mm using the Bortfelds relation in the range of 1 through 300 MeV we obtain the margin of error equal to 0.029 mm. The results thus correspond to the selected precision.

## Influence of inhomogeneities on the Bragg curve

We have already defined a one-dimensional Bragg curve in a water medium in such a way that it is directly possible to control the position of the peak based on the initial energy of protons. This section enhances the previous formulation to account for the changes of media and inhomogeneities.

Physicians have utilized the similarity of propagation of protons in water and in tissues. Subsequently, so called water equivalent (WET) has been introduced. WET is such a thickness of water that has the same effect on the loss of energy of proton beam as the specified thickness of another media in specific depth, see Figure 2.5.

Because the loss of the kinetic energy along the depth  $z$  is not constant, also the value of WET is dependent on the depth. Moreover, it is a function of the media and of its thickness.

Let us again begin with the Bragg-Kleeman rule, see Equation (2.1). We can thus approximately state the relation for kinetic energy of protons:

$$R_0 - z = \alpha E(z)^p \quad \Leftrightarrow \quad E(z) = \left( \frac{R_0 - z}{\alpha} \right)^{1/p}. \quad (2.7)$$

The above relation is considerably approximate, as it obviously neglects range straggling defined by Equation (2.2). It is thus not valid near the Bragg peak, but for the most of the depths it is sufficient. To acquire the energy with higher precision it can be directly computed by numerical integration of Bethe-Bloch equation (Olive et al., 2014):

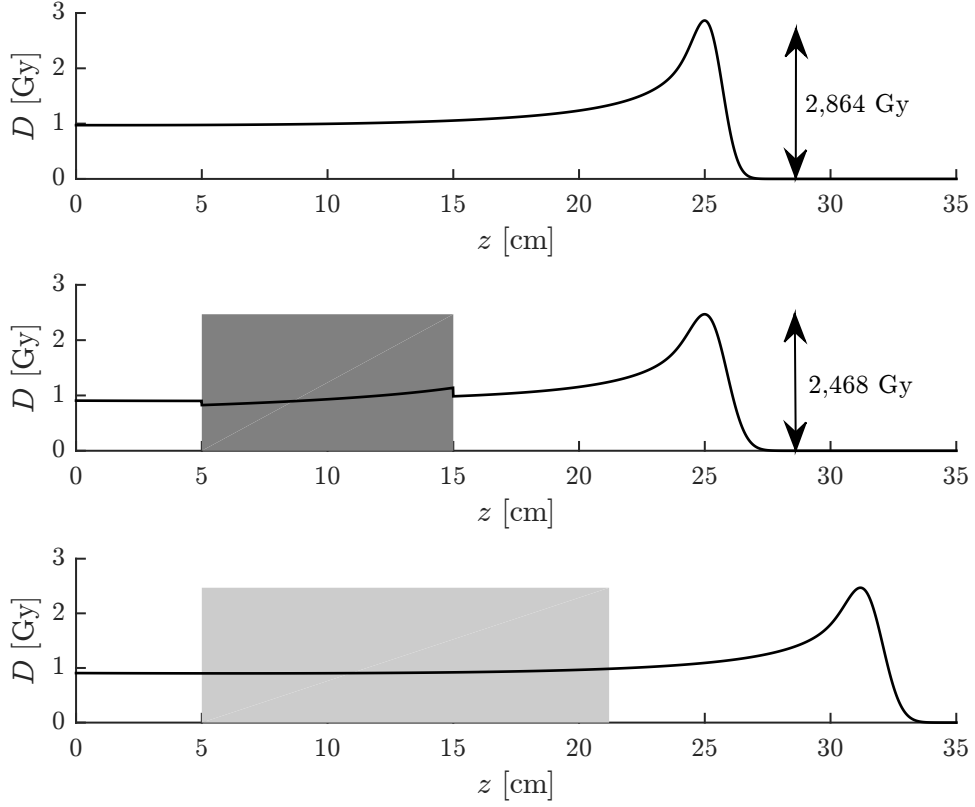


Figure 2.5: Influence of inhomogeneities on the shape of the Bragg curve. The upper Bragg curve has a peak located in the depth of 25 cm and propagates only through water medium. The middle Bragg curve has also a peak in the depth of 25 cm and propagates through water medium, but between the depths 5 through 15 cm we have placed a bone. The last Bragg curve represents a situation where the initial kinetic energy of the beam is equal to the middle Bragg curve but the medium is only water.

$$-\left\langle \frac{dE}{dz} \right\rangle = \frac{4\pi N_A r_e^2 m_e c^2 Z}{A} \frac{1}{\beta(E)^2} \left[ \frac{1}{2} \ln \frac{2m_e c^2 \beta(E)^2 \gamma(E)^2 T_{\max}}{I^2} - \beta(E)^2 \right], \quad (2.8)$$

where  $N_A$  denotes Avogadro's number, i.e. the number of particles in unit substance amount;  $r_e$  stands for classical electron radius,  $m_e$  denotes the mass of electron,  $c$  is the speed of light. Constant  $A$  denotes the atomic weight,  $Z$  states for atomic number.  $I$  denotes ionization energy. The maximal kinetic energy  $T_{\max}$  that can be transmitted from proton to a free electron in a single collision is computed (Olive et al., 2014) as

$$T_{\max} = \frac{2m_e c^2 \beta(E)^2 \gamma(E)^2}{1 + 2\gamma(E)m_e/m_p + (m_e/m_p)^2}, \quad (2.9)$$

where  $m_p$  stands for the mass of proton. All the remaining variables are functions of energy, hence the integration has to be performed iteratively.

Based on the theory of special relativity we can compute the velocity of protons (Evans, 2008)

$$\beta(E(z)) = \frac{v}{c} = \sqrt{1 - \frac{1}{\left(1 + \frac{E(z)}{m_p c^2}\right)^2}}, \quad (2.10)$$

and also the Lorentz factor  $\gamma$ :

$$\gamma = \sqrt{\frac{1}{1 - \frac{v^2}{c^2}}} = \sqrt{\frac{1}{1 - \beta(E)^2}}. \quad (2.11)$$

The water equivalent thickness is then formulated by modifying the Bethe-Bloch equation (2.8). The final form is then (Zhang – Newhauser, 2009):

$$WET(E) \approx t_w = t_m \left( \rho \frac{Z}{A} \left[ \ln \frac{2m_e c^2 \gamma(E)^2 \beta(E)^2}{I} - \beta(E)^2 \right] \right) \Big|_w^m, \quad (2.12)$$

where  $t_w$  denotes the water equivalent thickness,  $t_m$  the media thickness and  $\rho$  density.

The tissue does not consist of only one chemical element. To account for the real composition of tissues we will introduce a so called effective atom, i.e. effective atomic weight and number; and effective ionization energy of a slab or compound. The effective atomic weight is defined as (Hussein, 2003):

$$A_{\text{eff}} = \frac{\sum_{i=1}^n N_i A_i^2}{\sum_{i=1}^n N_i A_i}, \quad (2.13)$$

where  $n$  denotes the number of components of the compound,  $N_i$  states for the number of atoms of the  $i$ th component and  $A_i$  is the atomic weight of the  $i$ th component. The effective atomic number can be stated by equation (Hussein, 2003):

$$Z_{\text{eff}} = A_{\text{eff}} \sum_{i=1}^n \frac{N_i Z_i}{N_i A_i}, \quad (2.14)$$

where  $Z_i$  states for atomic number of the  $i$ th component.

The value of ionization energy  $I$  of specific component is uncertain, as it is difficult to measure. In the paper (Zhang – Newhauser, 2009) there is presented an approximate relation:

$$I = kZ, \quad (2.15)$$

$$k = \begin{cases} 14.5, & \text{for } Z \leq 8 \\ 13, & \text{for } 8 < Z \leq 13, \\ 11, & \text{for } Z > 13 \end{cases} \quad (2.16)$$

where  $Z$  denotes the atomic number of the specific chemical element and  $k$  is a constant dependent on the atomic number.

For compounds the following relation is used (Coderre, 2004):

$$\ln I_{\text{eff}} = \frac{\sum_{i=1}^n N_i Z_i \ln I_i}{\sum_{i=1}^n N_i Z_i}, \quad (2.17)$$

where  $I_i$  denotes the ionization energy of the  $i$ th component.

Due to the linear dependence of the water equivalent thickness on the thickness of the medium  $t_m$  in Equation (2.12) and due to the consideration that the kinetic energy is a function of depth  $z$ , it is obvious that the Bethe-Bloch equation is generally valid only for infinitesimally small thicknesses.

Therefore, we have divided the thickness of the medium into multiple smaller subintervals to ensure the required accuracy, see Table 2.1 for reference.

Medium	$E$ [MeV]	$t_m$ [mm]	$WET_{\text{exp}}$ [mm]	$WET_{\text{BK}}$ [mm]	$\text{Err}_{\text{exp-BK}}$ [%]	$WET$ [mm]	$\text{Err}_{\text{exp-WET}}$ [%]
Al	200	19.73	42.30	41.7	-1.42	41.861	-1.038
	200	14.90	32.20	31.5	-2.17	31.614	-1.820
	200	4.83	10.04	10.2	+1.59	10.249	+2.082
	100	14.90	31.50	31.1	-1.27	31.357	-0.454
	100	4.83	10.30	10.1	-1.94	10.166	-1.301

Table 2.1: Accuracy in the computation of WET.  $WET_{\text{exp}}$  denotes experimentally measured data for specified medium characteristics (Zhang et al., 2010),  $WET_{\text{BK}}$  states for the value computed according to (Zhang et al., 2010), the value  $WET$  denotes the WET computed based on the described theory.  $\text{Err}_{\text{exp-BK}}$  states the difference between  $WET_{\text{exp}}$  and  $WET_{\text{BK}}$ ,  $\text{Err}_{\text{exp-WET}}$  denotes the difference between  $WET_{\text{exp}}$  and  $WET$ .

## Multiple scattering theory

In the years of 1947 and 1948 Moliere has published a theory describing the effect of random collisions with ambient particles on the change of beam propagation direction. Gradually, Moliere introduced single scattering theory (Molière, 1947), which has been followed by the multiple scattering theory (Molière, 1948). Both the papers have been published only in German language. The English version has been created by H. A. Bethe (Bethe, 1953), who published an article *Moliere's Theory of Multiple Scattering*, where some generalizations valid for compounds have been omitted (Paganetti, 2012). Molier's theory of multiple scattering is considered as the most precise but concurrently the most complex, hence multiple trials have arose to simplify it.

Virgil L. Highland has introduced in the paper *Some practical Remarks on Multiple Scattering* (Highland, 1975) a simple Gaussian approximation while preserving the sufficient precision. Highland's approximation is, however, valid only for small thicknesses. Therefore, B. Gottschalk has generalized the formulation to account for thick targets (Gottschalk et al., 1993). The resulting equation is then

$$\theta_0 = 14.1q \left( 1 + \frac{1}{9} \log_{10} \frac{t}{L_R} \right) \times \left[ \int_0^t \left( \frac{1}{p(E)v(E)} \right)^2 \frac{dt'}{L_R} \right]^{1/2}, \quad (2.18)$$

where  $\theta_0$  denotes the characteristic multiple scattering angle, the constant  $q$  stands for the charge number of incident particle (i.e. in the case of protons  $q = 1$  eV),  $t$  denotes the thickness of medium and  $L_R$  the radiation length,  $p$  is the particle momentum and  $v$  the velocity. The velocity of the particle can be computed from the kinetic energy, see Equation (2.10). Similarly, the momentum of the particle is formulated as (Evans, 2008):

$$p(E) = \gamma(E)m_p v(E), \quad (2.19)$$

where  $\gamma$  denotes the Lorentz factor, see Equation (2.11), and  $m_p$  stands for the mass of a single proton. The last unknown variable, radiation length  $L_R$ , can be computed by equation (Gupta, 2010)

$$L_R = \frac{716.4}{Z(Z+1) \ln \frac{287}{\sqrt{Z}}}. \quad (2.20)$$

Because the tissues consist of multiple components we have to define again an effective atom. In the case of slabs the effective radiation length can be computed from the equation

$$\frac{t_0 \rho_0}{L_R} = \sum_{i=1}^n \frac{t_i \rho_i}{L_{R,i}}, \quad (2.21)$$

where  $\rho_i$  denotes the density of the  $i$ th slab,  $L_{R,i}$  is the radiation length of the  $i$ th slab,  $\rho_0$  denotes the effective density and  $t_0$  the total thickness. Simultaneously, the following equation is valid:

$$t_0 \rho_0 = \sum_{i=1}^n t_i \rho_i. \quad (2.22)$$

Similarly to slabs we can define effective atom for compounds:

$$\frac{A_{\text{eff}} N}{L_R} = \sum_{i=1}^n \frac{A_i N_i}{L_{R,i}}, \quad (2.23)$$

where  $n$  denotes the number of components of the compound and  $N$  states for substance amount.

Afterwards, we can finally approach to the calculation of the definite integral in Equation (2.18). In this thesis Newton's  $3/8$  method has been employed, see Appendix B. The literature (Gottschalk et al., 1993) does, similarly, mention the implementation of the Simpson's rule and a division of the thickness  $t$  based on the range  $R_0$ . The numerical comparison of both the approaches is shown in Table 2.2.

The 2-dimensional Gaussian distribution is stated as:

$$f(\theta) = \frac{1}{\sqrt{2\pi} \theta_0} e^{[-\frac{1}{2}(\frac{\theta}{\theta_0})^2]}, \quad (2.24)$$

where  $\theta$  is the multiple scattering angle, see Figure 2.6. By integration of the function  $f(\theta)$  in the interval  $(-\infty; \infty)$  we, of course, obtain 1. The 3-dimensional version of the Gaussian distribution is

$$f(\theta) = \frac{1}{2\pi\theta_0^2} e^{[-\frac{1}{2}(\frac{\theta}{\theta_0})^2]}. \quad (2.25)$$

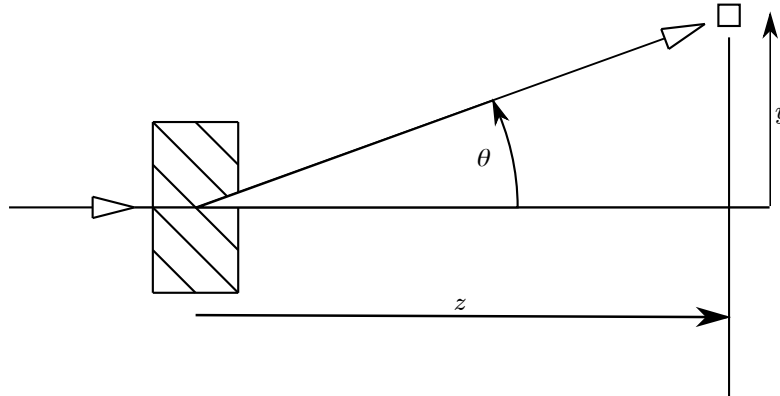


Figure 2.6: The dependence of the multiple scattering angle  $\theta$  on the depth  $z$  and on  $y$ .

Let us consider the proton beam propagates not only in the direction of depth  $z$  but also in the direction of orthogonal axis  $x$  and  $y$ . The geometry relation between the multiple scattering angle and 3-dimensional vector space is defined as

$$\tan \theta = \frac{\sqrt{x^2 + y^2}}{z}. \quad (2.26)$$

The resulting dose in an arbitrary location in space is then computed as

$$D(x, y, z) = D(z) \times \frac{1}{2\pi\theta_0^2} e^{\left[ -\frac{1}{2} \left( \frac{\arctan \frac{\sqrt{x^2 + y^2}}{z}}{\theta_0} \right)^2 \right]}. \quad (2.27)$$

Medium	Thickness <sup>4</sup> [g/cm <sup>2</sup> ]	$\theta_M$ [mrad]	$\theta_H$ [mrad]	Err <sub>M-H</sub> [%]	$\theta_0$ [mrad]	Err <sub>M-0</sub> [%]
Al	0.2160	3.701	3.534	-4.512	3.500	-5.431
	0.8170	8.051	7.670	-4.732	7.428	-7.738
	2.1729	13.880	13.104	-5.591	13.024	-6.167
	3.3500	16.920	16.258	-3.913	16.823	-0.573
	7.0960	28.357	26.931	-5.029	26.976	-4.870
	11.9570	42.065	39.986	-4.942	39.607	-5.843
	13.5690	42.422	40.534	-4.451	44.231	+4.271
	17.7230	61.129	58.230	-4.742	59.329	-3.092
	21.2450	91.129	87.103	-4.418	87.279	-4.225
	21.9150	92.504	88.657	-4.159	104.860	+16.600
	22.1100	98.021	93.645	-4.464	117.185	+19.551

Table 2.2: Comparison of accuracy in computation of the characteristic multiple scattering angle.  $\theta_M$  denotes the most accurate value computed by Moliér's theory of multiple scattering. The value  $\theta_H$  is given in (Gottschalk et al., 1993) as a result of Highland's approximation. The angle  $\theta_0$  represents values computed by implementation according to this thesis. Err<sub>M-H</sub> denotes the percentage difference between  $\theta_M$  and  $\theta_H$ , Err<sub>M-0</sub> states for the percentage difference between  $\theta_M$  and  $\theta_0$ .

<sup>4</sup>The physical units of thickness are usually g/cm<sup>2</sup>, i.e. the actual thickness multiplied by density of the medium.



## Chapter 3

# Multi-objective programming

### Formulation of multi-objective programming

Multi-objective programming is a specific task of mathematical programming in which there exist multiple conflicting objective functions optimized simultaneously. In reality these tasks are very common. As an example one can use a purchase of a car – although there is a need to maximize technical conditions and accessories of a car one tends to minimize costs for the purchase. If it was considered only the first aspect (or objective), the object of the consequent purchase would have probably been a new sports car with costs exceeding \$200 000. In the case of only considering the second objective – costs – one would end with a cheap car wreck. Nevertheless, none of these solutions is in fact appropriate. The following pages try to describe how to choose a solution that is appropriate to all the objective functions.

The problem can be generally defined as

$$\begin{aligned} \min [f_1(x), \dots, f_q(x)], \\ x \in \chi, \end{aligned} \tag{3.1}$$

where  $x$  stands for design variables in  $n$ -dimensional design space  $\chi \subseteq \mathbb{R}^n$ . Similarly, objective functions  $f(x)$  form  $q$ -dimensional objective space  $\Upsilon \subseteq \mathbb{R}^q$ . The shape of the design space is usually specified implicitly by constraints.

$$\begin{aligned} \chi := \{x \in \mathbb{R}^n : g(x) \leq 0, \\ h(x) = 0\}. \end{aligned} \tag{3.2}$$

### Dominated and non-dominated solution

By fulfilling the constraints given in Equation (3.2) we obtain two sorts of solutions (Jablonský, 2002).

Let there exist feasible solutions  $x^{(0)}, x^{(1)} \in \chi$ :

- Feasible solution  $x^{(1)}$  dominates to feasible solution  $x^{(0)}$  if for all objective functions  $f_j(x)$ ,  $j \in \{1, \dots, q\}$  applies  $f_j(x^{(1)}) \leq f_j(x^{(0)})$  and at least for one objective function  $f_k(x)$  applies

$$f_k(x^{(1)}) < f_k(x^{(0)}).$$

- If there does not exist any  $x^{(1)}$  for which implies  $x^{(1)}$  dominates  $x^{(0)}$  then  $x^{(0)}$  is called non-dominated or Pareto-optimal solution.

This specifically means that there does not exist any feasible solution having all objective function values better (i.e. lower) than for any non-dominated solution.

### Pareto set and Pareto surface

The set of all feasible non-dominated design variables is called Pareto set. Similarly, the set of all feasible non-dominated objective function values is called Pareto surface.

According to the shape we can distinguish between convex and non-convex Pareto set or Pareto surface, for comparison see Figure 3.1.

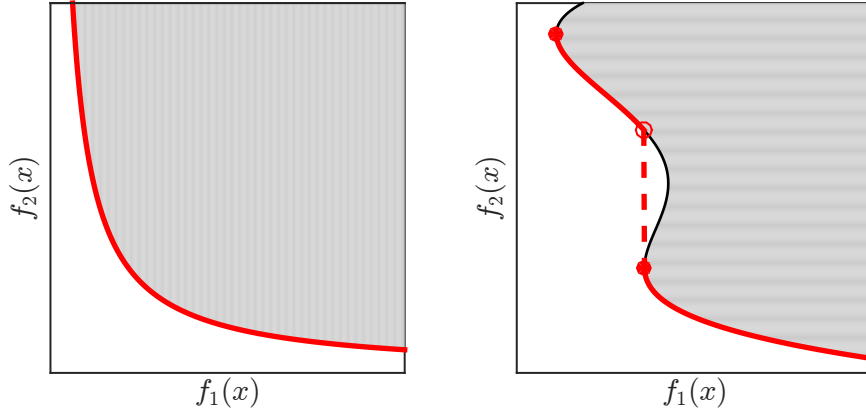


Figure 3.1: Shape of Pareto surface. The left figure shows convex Pareto surface; the right figure shows non-convex Pareto surface. Feasible objective space  $\Upsilon$  is drawn in a gray color. Pareto optimal solutions are rendered as red.

### Multi-objective linear programming

If all the constraints  $g(x)$  and  $h(x)$  from Equation (3.2) and concurrently all the objective functions  $f(x)$  from Equation (3.1) are linear, then it is possible to solve such problem by multi-objective linear programming (MOLP).

Gale, Kuhn, Tucker (1951) considered a general linear program with a matrix objective function and introduced theorems of existence and duality. Due to the fact that vector and scalar objective functions are a special case of this program, this theory is generally considered as a base for linear programming (Luptáčík, 2009).

A multi-objective linear program can be written in the form

$$\begin{aligned} \min Cx : \quad & Ax \leq b, \\ & l_b \leq x \leq u_b, \end{aligned} \tag{3.3}$$

where  $C$  denoted the matrix of objective functions, with size  $n \times q$  and each row representing one objective function. Constraints are specified by matrix  $A$  with the size  $m \times n$  and by a column vector  $b$  of length  $m$ . Constant  $m$  stands for the count of constraints. Design variables  $x$  can be bounded by a lower bound  $l_b$  or by an upper bound  $u_b$ .

The aim of addressing a MOLP problem is usually obtaining a particular non dominated solution, eventually acquiring the whole Pareto set, because there does not frequently appear a situation with a feasible globally optimal solution that is valid for all objective functions simultaneously. To solve a MOLP problem it is possible to use several approaches. Some of them are described in the following text.

### Aggregation of objective functions

Aggregation of objective functions is a method based on evaluation of individual objective functions by weights  $w$  followed by an assembly of aggregated objective function. The weights have to be nonzero and positive. In many cases a condition that the total sum of weights is equal to one is also added (Jablonský, 2002).

To permit aggregation of all the objective functions it is needed to unify their units, i.e. normalize them.

#### Example

Let us assume a MOLP defined by Equation (3.3) and the following matrices:

$$C = \begin{pmatrix} 1 & 0 \\ 0 & 1 \end{pmatrix}, \quad A = \begin{pmatrix} -3 & -3 \end{pmatrix}, \quad b = \begin{pmatrix} -5 \end{pmatrix}, \quad l_b = 0, \quad u_b = 3. \quad (3.4)$$

The problem can be divided into two subproblems according to the objective functions:

$$\begin{array}{ll} \min z_1 = x_1 & \min z_2 = x_2 \\ -3x_1 - 3x_2 \leq -5 & -3x_1 - 3x_2 \leq -5 \\ 0 \leq x_1 \leq 3 & 0 \leq x_1 \leq 3 \\ 0 \leq x_2 \leq 3 & 0 \leq x_2 \leq 3 \end{array} \quad (3.5)$$

The solution of the first subproblem is a point  $[0; \frac{5}{3}]^T$  and of the second subproblem a point  $[\frac{5}{3}; 0]^T$ . According to these two solutions it is possible to define a range of values of Pareto-optimal objective functions – both are  $\langle 0; \frac{5}{3} \rangle$ . Objective functions should be further normalized – each objective function is divided by the length of the corresponding range of values of Pareto-optimal objective function. In this particular example we can then write:

$$z_1 = \frac{x_1}{\frac{5}{3}} = \frac{3}{5}x_1 \quad z_2 = \frac{x_2}{\frac{5}{3}} = \frac{3}{5}x_2. \quad (3.6)$$

If there was not any information about the problem in advance the selection of weights  $w_1$  and  $w_2$  would be random. For this example it was chosen that  $w_1 = 0.3$  and  $w_2 = 0.7$ . The condition of the cumulated sum equal to 1 is also fulfilled. Let us now assemble the aggregated objective function:

$$C_{\text{agg}} = w_1 \times \left(\frac{3}{5}x_1 + 0x_2\right) + w_2 \times \left(0x_1 + \frac{3}{5}x_2\right) = 0.18x_1 + 0.42x_2. \quad (3.7)$$

By considering an aggregated objective function  $C_{\text{agg}}$  the optimal solution is a point  $[\frac{5}{3}; 0]^T$ .

According to the shape of the polytope defining feasible values of objective functions (see Figure 3.2) it is possible to determine that for  $w_1 \in \langle 0; 0.5 \rangle$  and  $w_2 \in \langle 0.5; 1 \rangle$  the globally optimal solution will always be just computed point  $[\frac{5}{3}; 0]^T$ . Otherwise, if  $w_1 \in \langle 0.5; 1 \rangle$  and  $w_2 \in \langle 0; 0.5 \rangle$ , the globally optimal solution will be the point  $[0; \frac{5}{3}]^T$ . If both the weights are equal, i.e.  $w_1 = w_2 = 0.5$ , the solution is defined as an edge connecting both the above listed points. According to the used algorithm usually a vertex is obtained<sup>1</sup>.

The benefit of solving MOLP by aggregation of objective functions is mainly its simplicity. In case of the need to get higher count of non-dominated solutions this method is not so useful because it is difficult to determine relevant values of weights  $w$  to attain different non-dominated solutions. This is however significant in more complex problems.

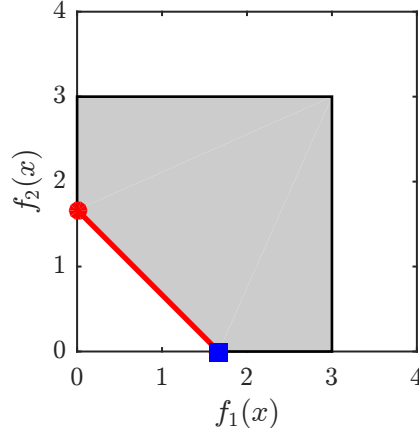


Figure 3.2: The shape of Pareto surface. Objective space (here identical to design space) is colored with gray. Non-dominated solutions are drawn by red line.

### Compromise solution according to the maximal component

Considering compromise solution according to the maximal component  $\delta$  approach we are searching a non-dominated solution that minimizes the maximal (worst) component (objective). In the case of maximization the minimal component should be maximized (Jablonský, 2002).

#### Example

Let us consider the same example defined by Equation (3.4). The normalized matrix of objective functions is

$$C_{\text{norm}} = \begin{pmatrix} \frac{3}{5} & 0 \\ 0 & \frac{3}{5} \end{pmatrix}. \quad (3.8)$$

We will now reformulate the initial linear program and introduce the maximal component  $\delta$ :

<sup>1</sup>Simplex and dual-simplex algorithms always return a vertex of the polytope. Interior-point method can return any point located on the edge.

$$\begin{aligned}
\min \delta : \{ & C_{\text{norm}} x \leq \delta, \\
& Ax \leq b, \\
& x \geq 0, \\
& \delta \geq 0 \}.
\end{aligned} \tag{3.9}$$

Solving the above problem considering the weights of individual objective functions  $w_1 = 0.5$  and  $w_2 = 0.5$ , we obtain the maximal component  $\delta = \frac{5}{6}$  and a solution  $[\frac{5}{6}; \frac{5}{6}]^T$ , see Figure 3.3, where the optimal solution is rendered as a blue square. The maximal deviation of the values of objective functions is

$$(1 - \delta) \times 100 = 16.7\%. \tag{3.10}$$

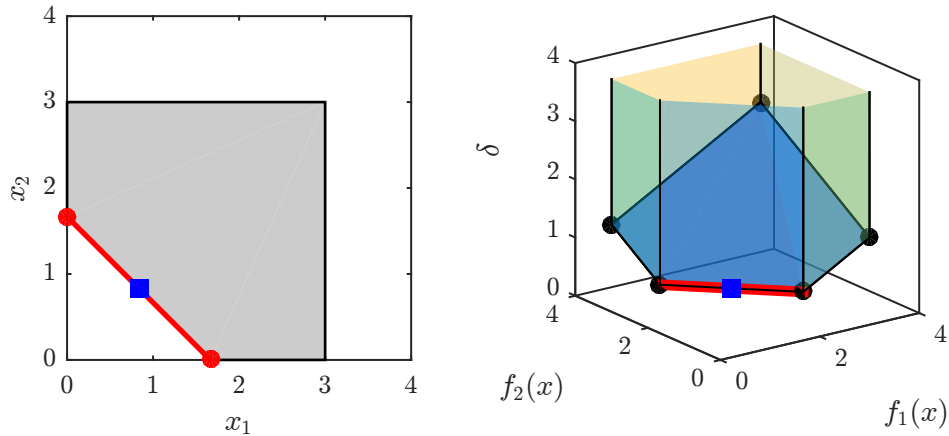


Figure 3.3: Compromise solution according to maximal component. Pareto-optimal solution are displayed in a thick red line.

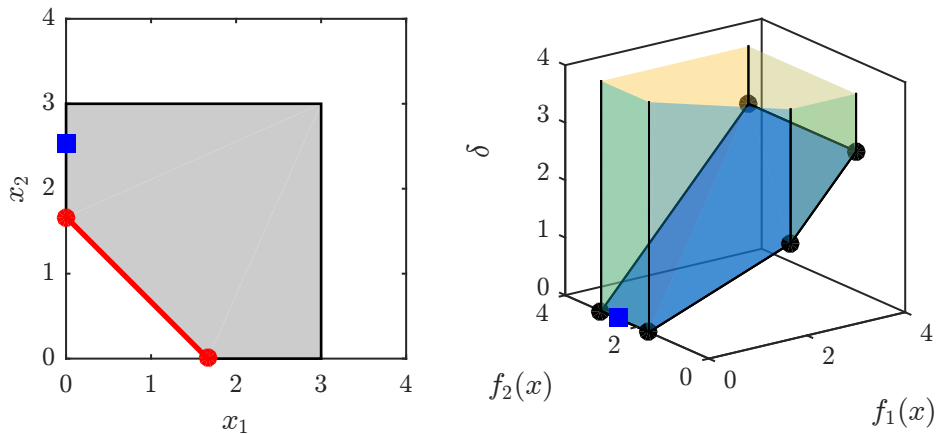


Figure 3.4: Compromise solution according to maximal component – dominated solution.

The variation of weights then enables us to rotate the polytope defining the objective space along the variable, whose weight has been changed, see the right image in Figure 3.3. Similarly to the previous case we obtain a point  $[0; \frac{5}{3}]^T$  using the weights  $w_1 \in (0; 0.5)$  and  $w_2 \in (0.5; 1)$ . Weights

in interval  $w_1 \in (0.5; 1)$  and  $w_2 \in (0; 0.5)$  lead to an optimal solution  $[\frac{5}{3}; 0]^T$ . If  $w_1 = w_2 = 0.5$  the optimal solution set is defined by the whole edge of the polytope. It should be noted, however, that in the case that one weight is equal to 1 and the other is equal to 0, we can easily obtain a dominated solution not located on Pareto surface as shown in Figure 3.4.

### Minimization of the distance from ideal values

The method of minimization of the distance from ideal values searches a compromise solution that minimizes the weighted sum of deviations from ideal values of individual objective functions.

The ideal values of individual objective functions are denoted by  $z_1^{\text{opt}}, z_2^{\text{opt}}, \dots, z_q^{\text{opt}}$ , respectively. Their values can be obtained solving the MOLP defined by Equation (3.3) independently for all of the objective functions (Jablonský, 2002).

#### Example

Let us consider a linear program defined by Equation (3.4). We have also chosen  $w_1 = 0.6$  and  $w_2 = 0.4$  as the weights of objective functions.

Firstly, we compute the ideal values, i.e. the optimal values for individual objectives. Thus, we obtain the points  $z_1^{\text{opt}} = [0; \frac{5}{3}]^T$  and  $z_2^{\text{opt}} = [\frac{5}{3}; 0]^T$ . Note that in this case the design space is equal to the objective space.

Afterwards, the objective functions are normalized:

$$C_{\text{kom}} = \sum_{i=1}^q w_i (c_i x - z_i^{\text{opt}}) = 0.6 \times \left( \frac{x_1}{5} - \frac{0}{5} \right) + 0.4 \times \left( \frac{x_2}{5} - \frac{0}{5} \right) = 0.36x_1 + 0.24x_2. \quad (3.11)$$

Consequently, we will solve a simple linear program:

$$\begin{aligned} \min C_{\text{kom}} : \{ & Ax \leq b, \\ & x_1, x_2 \geq 0 \}, \end{aligned} \quad (3.12)$$

which yields an optimal solution  $[0; \frac{5}{3}]^T$ , see Figure 3.5, where the optimal solution is drawn as a blue square.

The advantage of the presented approach is the ability to obtain solutions that are balanced (in objective functions), especially when the Pareto surface is rugged. The drawback is, however, that the optimal solution is still dependent on properly chosen weights. Also, to preserve the linearity in the problem formulation only the weighted sums of individual components of distance vector are minimized and not the real scalar value of the length.

### Goal programming

The base of goal programming are goals stating multiple target values we want to achieve. According to (Jablonský, 2002) goals can be divided into:

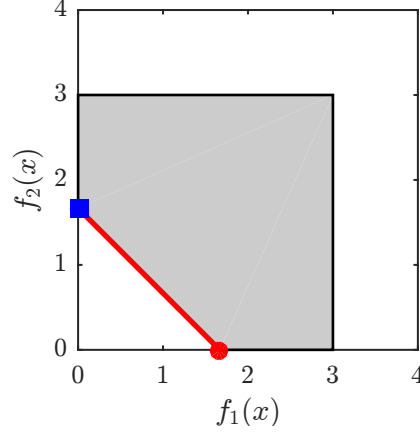


Figure 3.5: The shape of the objective space of the presented example of minimization of the distance from ideal values. The red color represents Pareto-optimal solutions.

- **Fixed goals** express a constraint that have to be fulfilled (hard constraints). If it is impossible to satisfy fixed goals the solution of linear program is infeasible, i.e. a feasible design set is empty. Fixed goals are written in form of constraints:

$$Ax \leq b. \quad (3.13)$$

- **Free goals** are constraints (mild constraints) expressing specific balance levels between left and right side of (in)equalities. The deviations are in forms of *negative deviational variable*  $\delta^-$  and *positive deviational variable*  $\delta^+$ . Negative deviational variable represents the level by which the target level is under-achieved. Positive deviational variable represents the level by which the target level is over-achieved (Jones – Tamiz, 2010, pg. 11). Both the deviational variables are constrained to be non-negative. It is then possible to write:

$$Ax \leq b + \delta^+ - \delta^-. \quad (3.14)$$

In goal programming the objective function connects all the deviational variables and is usually written in form of an *achievement function* minimizing the cumulated sum of all deviational variables. Other used objectives minimize the maximal deviation or a weighted sum of all deviations to express their importance.

### Example

Assumed MOLP is written in form:

$$\max Cx : \quad Ax \leq 0. \quad (3.15)$$

$$C = \begin{pmatrix} 1 & 0 \\ 0 & 1 \end{pmatrix}, \quad A = \begin{pmatrix} 1 & 3 \\ 2 & 1 \end{pmatrix}, \quad b = \begin{pmatrix} 4 \\ 5 \end{pmatrix}, \quad x_1 \geq 0, \quad x_2 \geq 0. \quad (3.16)$$

Ideal (or target) value is considered to be an optimum of each individual objective. By solving the

LP with the first objective the optimal solution is  $[2.5; 0]^T$ . While evaluating the second objective the solution of the same LP is  $[0; \frac{4}{3}]^T$ . Therefore the unfeasible ideal solution is a point with coordinates  $[2.5; \frac{4}{3}]^T$ .

The goals are then expressed in the form of deviational variables and the MOLP is thus rewritten to:

$$\begin{aligned} \min (\delta_1^- + \delta_2^-) : \quad & \{Ax \leq b, \\ & x_1 = 2.5 - \delta_1^-, \\ & x_2 = \frac{4}{3} - \delta_2^-\}. \end{aligned} \quad (3.17)$$

The resulting compromise solution is a point  $[2.2; 0.6]^T$ ; values of deviational variables are  $\delta_1^- = 0.3$  a  $\delta_2^- = 0.733$ , see Figure 3.6.

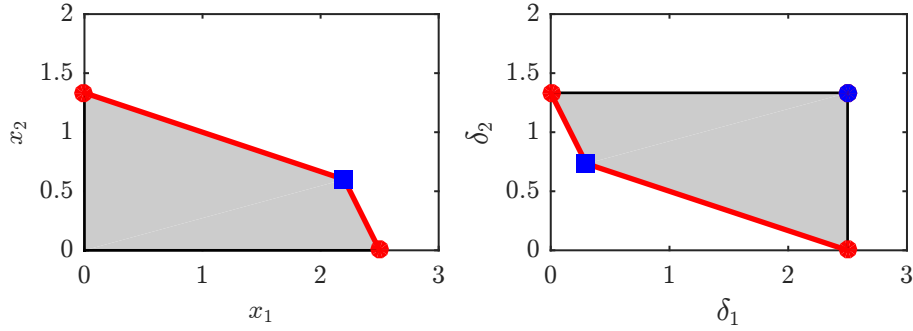


Figure 3.6: The shape of design space and objective space formed by deviational variables. Red color indicates Pareto-optimal solutions.

### Benson's algorithm

Benson's algorithm is based on the assumption that if the total count of objectives is significantly lower than the count of design variables, i.e.  $q = \dim(\Upsilon) \ll n = \dim(\chi)$ , it is assumed that multiple points located on Pareto set  $\chi_E$  will be projected into one point located on Pareto surface  $\Upsilon_E$ . Because of this reason Benson have considered that obtaining Pareto surface should be significantly less computationally demanding than obtaining Pareto set (Benson, 1998).

The decision maker also chooses the specific compromise Pareto-optimal solution mainly based on objectives' values, it is therefore not important to obtain the whole Pareto set. Benson therefore suggested a method to solve MOLP in the objective space.

Let's consider there exist a Pareto surface  $\Upsilon_E$  (i.e. a set of all compromise solutions in objective space) and a set of all feasible solutions in objective space  $\Upsilon \subseteq \mathbb{R}^q$ . It is then possible to choose  $\Upsilon'$  such that  $\Upsilon_E \subseteq \Upsilon' \subset \mathbb{R}^q$ . The polytope  $\Upsilon'$  has to be bounded<sup>2</sup>.

Subsequently it is possible to compute an interior point  $p$  of polytope  $\Upsilon$  and an ideal point  $y_I$ , which is defined as:

<sup>2</sup>In case that the objective space is not bounded it is needed to create such artificial constraints to bound the polytope that the output of optimization is not affected.



$$y_I = \min\{y : y \in \Upsilon'\}. \quad (3.18)$$

The ideal point is not located in the polytope  $\Upsilon$ , it has a lower value than all feasible members of the polytope:  $y_I < y \in \Upsilon$ . One can then build a vector  $\overrightarrow{py_I}$  connecting the interior point with the ideal point and find a minimal scalar  $\rho \in (0,1)$ , such that

$$\min(\rho) : p + \rho \times \overrightarrow{py_I} \geq Cx. \quad (3.19)$$

Because of the fact that the shape of feasible objective space and subsequently also the shape of Pareto surface is always convex<sup>3</sup> there does exist only one non-dominated solution.

The basis for the next part is a pair of primal and dual LPs:

$$P(y) = \min(z) : \quad Ax \leq b, \quad Cx - z \leq y, \quad (3.20)$$

$$D(y) = \min(b^T u + y^T w) : \quad A^T u + C^T w \leq 0, \quad \sum w \geq 1, \quad u \geq 0, \quad w \geq 0. \quad (3.21)$$

Dual solution of the primal problem (3.20) or the primal solution of the dual problem (3.21) yields values of dual variables  $u$  and  $w$ , which are used to build a cutting (hyper)plane defined as

$$\mathcal{H}(u, w) = \{y \in \mathbb{R}^q : \langle w, y \rangle = \langle b, u \rangle\}. \quad (3.22)$$

Cutting hyperplanes  $\mathcal{H}$  subsequently crop the polytope  $\Upsilon'$  so the initial condition  $\Upsilon_E \subseteq \Upsilon'$  is still valid. The shape of polytope  $\Upsilon'$  is saved in a form of linear inequalities. Considering that the shape of the initial polytope  $\Upsilon'$  is described by inequalities  $A'y \leq b'$ , then the cropped polytope is updated to

$$\begin{bmatrix} A' \\ -w \end{bmatrix} y \leq \begin{bmatrix} b' \\ b^T u \end{bmatrix}. \quad (3.23)$$

From the above linear constraints (3.23) it is possible to obtain all vertices  $s$  of the polytope. According to (Shao et al., 2008) we can use the on-line vertex enumeration approach described in (Chen et al., 1991). In this thesis we have, however, used an already written function `con2vert` by Michael Kleder (Kleder, 2005).

The vertices  $s$  are divided into two groups: vertices inside  $\Upsilon$  and vertices not inside  $\Upsilon$ . Vertices that are solving the initial LP, i.e. the first group, are also members of  $\Upsilon_E$  – they are Pareto-optimal solutions. Vertices in the second group that are not solving the initial LP are used as a repetitive input into (3.19) instead of the ideal point  $y_I$ . The described algorithm is repeated until all vertices  $s$  are members of  $\Upsilon$  and the whole shape of Pareto surface is thus obtained.

It is proven that the iteration count of Benson's algorithm is finite. According to (Shao et al., 2008) it is possible to introduce an approximate solution of Benson's algorithm gaining a significant speedup. This modification is however not used in this thesis.

---

<sup>3</sup>Because the constraints of LP are linear.

### Parallelization of Benson's algorithm

In a recent decade there have been a significant growth in the spread of multi-core processors, which subsequently led into the possibility of parallelization of algorithms. An ideally parallelized algorithm gain a speedup linear to the number of processors.

Benson's algorithm consists of the main iteration **while** cycle. Inside the **while** cycle there are two **for** cycles:

- **Cycle 1:** Computation of non-dominated solutions in directions defined by vectors  $\vec{sp}$ , see Equation (3.19), and subsequent construction of cutting hyperplanes, see Equation (3.20) or (3.21).
- **Cycle 2:** A check that the computed vertices  $s$  of the polytope  $\Upsilon'$  are solutions of the initial LP, i.e. are located in  $\Upsilon$ .

An important assumption for parallelization of the algorithm is a mutual independence within individual mathematical operations. Because the above condition is satisfied and also the count and the size of output variables is known in advance, it is an ideal part of the algorithm to be parallelized.

In MATLAB environment the algorithm has been parallelized by the usage of two **parfor** cycles.

### Example

An MOLP example is defined by Equation (3.3) and by the following matrices:

$$C = \begin{pmatrix} 1 & 0 \\ 0 & 1 \end{pmatrix}, \quad A = \begin{pmatrix} -2 & -1 \\ -1 & -3 \\ -3 & -3 \end{pmatrix}, \quad b = \begin{pmatrix} -2 \\ -2 \\ -4 \end{pmatrix}, \quad x_1, x_2 \geq 0. \quad (3.24)$$

As the ideal point in the objective space it was computed the point  $y_0^I = (0; 0)^T$  because of the condition of non-negative values of both the variables. Also, we computed an arbitrary interior point, e.g.  $p = (2; 2)^T$ .

This specific MOLP does not however specify any upper bound, thus the polytope  $\Upsilon'$  is not bounded, i.e.  $f_1(x) \in \langle 0; \infty \rangle$  and  $f_2(x) \in \langle 0; \infty \rangle$ . To upper-bound the objective space we add the constraints

$$\forall f(x) \leq 1000, \quad (3.25)$$

which do not influence the shape of Pareto surface. Subsequently, we build the polytope  $\Upsilon'$  containing the Pareto surface  $\Upsilon_E$ :

$$\Upsilon' : \left\{ \begin{array}{l} 0 \leq f_1(x) \leq 1000, \\ 0 \leq f_2(x) \leq 1000 \end{array} \right\}. \quad (3.26)$$

In the first iteration we solve Equation (3.19) and thus obtain a scalar  $\rho = \frac{2}{3}$ . Consequently, we can compute  $y_1 = (\frac{2}{3}; \frac{2}{3})^T$ .

Solving Equation (3.21) we get dual variables  $u = (\frac{1}{3}; 0; 0; 0; 0)^T$  and  $w = (\frac{2}{3}; \frac{1}{3})^T$ . According to Equation (3.23) the shape of the polytope  $\Upsilon'$  is updated (see the second iteration in Figure 3.7):

$$\Upsilon' : \left\{ \begin{array}{l} \forall f(x) : 0 \leq f(x) \leq 1000 \\ -\frac{2}{3}f_1(x) - \frac{1}{3}f_2(x) \leq -\frac{2}{3} \end{array} \right\}. \quad (3.27)$$

The updated polytope consists of vertices  $s$  and the upper-bounding vertices are removed. For all remaining vertices  $s$  it is checked whether they are located in the set of all feasible solutions in the objective space:

$$\min[0; 0] : \{Ax \leq b, C = s\}. \quad (3.28)$$

If Equation (3.28) is feasible, then the vertex  $s$  (i.e. in this case the point  $[0; 2]^T$ ) is a non-dominated solution of the initial MOLP. Otherwise if the LP is infeasible, the algorithm is run again with  $y_I = s$ , scalar  $\rho$  is computed etc.

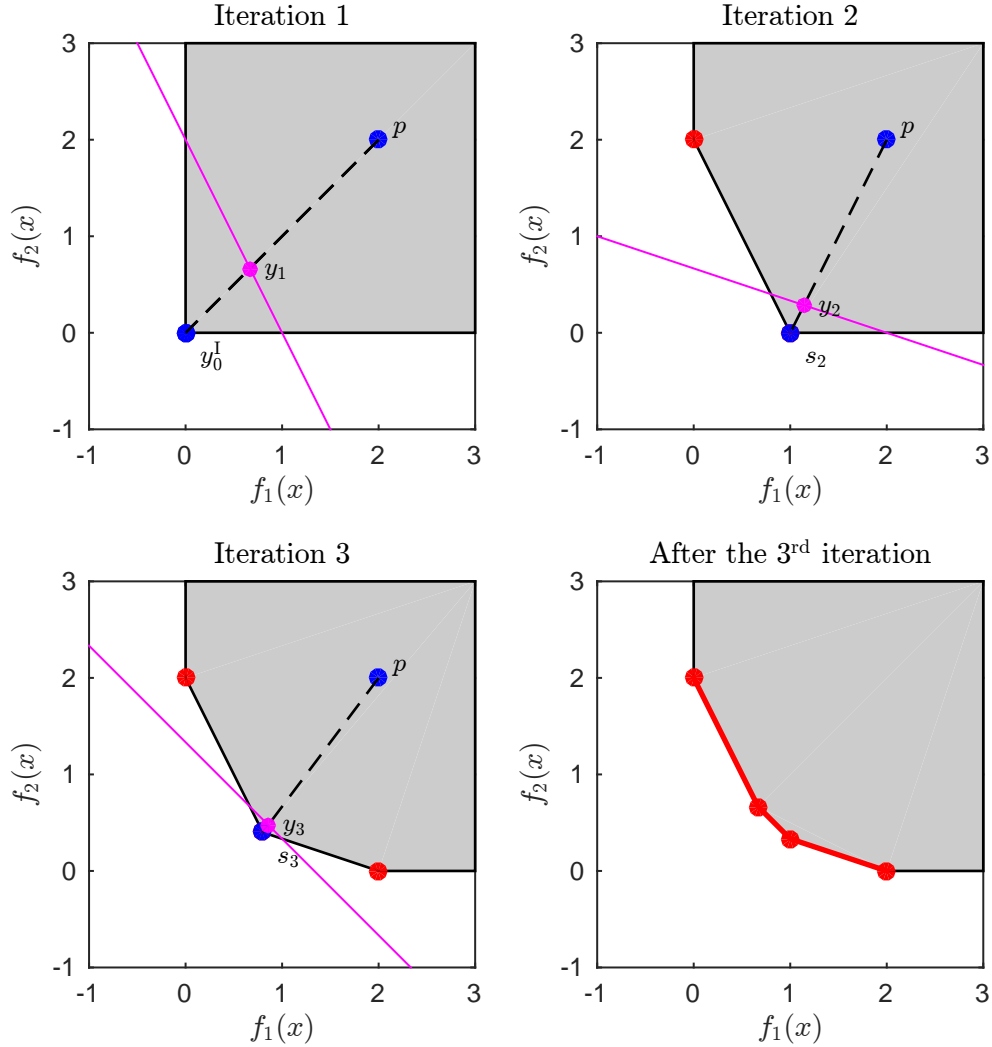


Figure 3.7: Sample iteration progress of Benson's algorithm applied on a simple example.

In the subsequent iterations we obtain all the vertices defining the Pareto surface:  $[0; 2]^T$ ,  $[1; \frac{1}{3}]^T$ ,  $[\frac{2}{3}; \frac{2}{3}]^T$  and  $[2; 0]^T$ .

The algorithm terminates only if all the vertices  $s$  are in the polytope  $\Upsilon$ , i.e. the whole Pareto surface is found (see the condition after the third iteration in Figure 3.7).

### Non-dominated solutions uniformly distributed on the Pareto surface

The decision maker cannot, however, visit the infinite amount of solutions defining the Pareto surface. Therefore, we have developed an algorithm to compute uniformly distributed solutions on the Pareto surface, describing thus its inner approximation.

According to Equation (3.19) it is possible to find a non-dominated solution in a direction specified by the vector  $\overrightarrow{py_I}$ . By solving the above equation for different directions we obtain unique Pareto-optimal solutions, that are located either in vertices, edges or facets of the polytope.

At first it is needed to obtain border points defining the shape of the Pareto surface. The border points are the extreme points of the Pareto surface, e.g. their all except one coordinates are equal to zero. Consequently, it is possible to construct a hyperplane defined by the extreme points.

The hyperplane then forms two half-spaces, one containing the ideal point  $y_I$  and the other containing the anti-ideal point (or in the case of an unbounded problem the unbounded solution). Therefore, if we add a constraint defining the half-space containing the anti-ideal point to the original MOLP, the whole Pareto surface will be cut off. Although the solution of such a problem is not anyhow useful for the treatment itself, it is ensured that if we solve the modified problem by Benson's algorithm it will be very fast (it will take exactly 2 iterations). The convex hull of the resulting vertices then describes the actual shape of the Pareto surface.

Let us now consider the hyperplane constrained by a convex hull obtained by Benson's algorithm. On the resulting facet a random point generator, see (Devroye, 1986) and (Myšáková, 2013), generates random distribution of points. Due to the randomness of their location it is needed to ensure their uniform distribution. In this thesis we have used a modified version of the algorithm `distmesh`, see Appendix A or (Tyburec, 2014a). The used algorithm secures that the resulting distribution is uniform.

In the following step the ideal point is computed. According to Equation (3.19) we build direction vectors  $\overrightarrow{py_I}$  connecting the uniformly distributed points  $p$  on the hyperplane and the ideal point  $y_I$ . By solving the LP (3.19) we obtain non-dominated solutions, i.e. points on the Pareto surface. By computation of the convex hull defined by the uniformly distributed non-dominated solutions we obtain an inner approximation of the Pareto surface with all the points located exactly on the Pareto surface.

#### Example

Let us consider a MOLP described by Equation (3.3) and the matrices:

$$C = \begin{pmatrix} 1 & 0 & 0 \\ 0 & 1 & 0 \\ 0 & 0 & 1 \end{pmatrix}, \quad A = \begin{pmatrix} -3 & -2 & -5 \\ -2 & -1 & -1 \\ -1 & -1 & -3 \\ -5 & -2 & -4 \end{pmatrix}, \quad b = \begin{pmatrix} -55 \\ -26 \\ -30 \\ -57 \end{pmatrix}, \quad \forall x \geq 0. \quad (3.29)$$

A consecutive solution of the MOLP with objectives  $C_1 = (10^{-6}; 1; 1)^T$ ,  $C_2 = (1; 10^{-6}; 1)^T$  and  $C_3 = (1; 1; 10^{-6})^T$  leads to the maximal values of the Pareto-surface:  $[30; 0; 0]^T$ ,  $[0; 30; 0]^T$  and  $[0; 0; 26]^T$ . All these points are drawn in black in Step 1 in Figure 3.8. The above three points also define a plane (see Step 1 in Figure 3.8):

$$x + y + \frac{15}{13}z - 30 = 0. \quad (3.30)$$

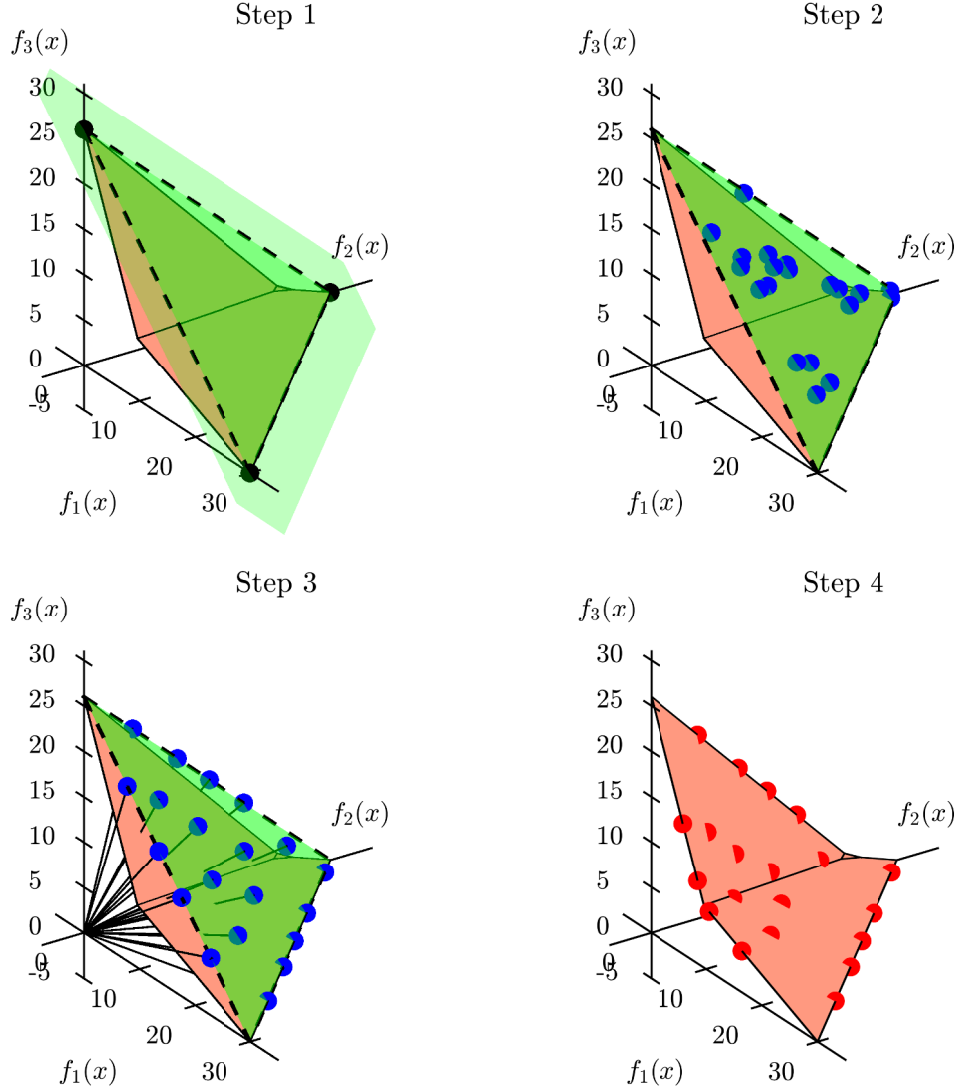


Figure 3.8: Solution process of obtaining uniformly distributed solutions on Pareto surface.

The equation defining the plane is then added to the initial MOLP:

$$-x - y - \frac{15}{13}z \leq -30 \quad (3.31)$$

Note that the ideal point  $y_I = [0; 0; 0]$  is not solving Equation (3.31). The MOLP defined by (3.29) and (3.31) is solved by Benson's algorithm, from which the convex hull defining the feasible objective space is obtained.

On the resulting facet random points are generated (see Step 2 in Figure 3.8). The uniformity is

secured by the usage of algorithm **distmesh**. Uniformly distributed points on the plane and the ideal point  $y_I$  form direction vectors  $\overrightarrow{py_I}$  (see Step 3 in Figure 3.8).

Finally, for each vector  $\overrightarrow{py_I}$  Equation (3.19) is solved and the unique Pareto-optimal solution (see Step 4 in Figure 3.8) is found.

Generation of convex hull defined by just computed Pareto-optimal solutions then yields an inner approximation of the Pareto surface.

## Chapter 4

# Optimization of proton therapy treatment plan

A proton therapy treatment plan is a certain recipe defining from which direction(s) and by what intensity the patient should be irradiated. Firstly, a 3-dimensional model of tissues surrounding the tumor is obtained using computed tomography (CT) or magnetic resonance (MRI).

Radiation oncologists then mark all volumes of interest (VOI) – Organs at Risk (OARs) and the tumor (TAR) – by contour lines. The aim of the irradiation is to deliver such a dose  $D_{\text{TAR},\min}$  to the tumor, that the cancer cells are destroyed or sufficiently damaged (Hynková, Doleželová, Šlampa). It is also usually not possible to avoid irradiation of surrounding healthy tissues. To reduce the number of constraints in the optimization problem formulation, i.e. to avoid prescribing a maximal dose for normal tissues, it is usually defined a specific maximal dose in the tumor  $D_{\text{TAR},\max}$  (Petit, Seco, Kooy, 2013), having the similar effect. For OARs it is defined a maximal dose  $D_{\text{OAR},\max}$ , such that the damages and the long-term consequences of irradiation on the critical organs are limited.

### Formulation of the optimization problem

In the direction of the propagation of radiation, i.e. in the depth  $z$ , the dose can be described by Equation (2.3), which shows that the dose  $D$  is linearly dependent on the primary fluence  $\Phi_0$ . In other words it is possible to write

$$d_j = \sum_{i=1}^n \Phi_{0,ij} D_{ij}^*, \quad (4.1)$$

i.e. the dose in voxel  $j$  is equal to the contribution of  $n$  individual beams. The dose  $D_{ij}^*$  stands for the dose caused by one particle.

### Objective function

In the literature several objective functions are used. Most commonly, a quadratic objective function is used (Pflugfelder et al., 2008):

$$F(\Phi_0) = \frac{1}{N_{\text{TAR}}} \sum_{l=1}^{N_{\text{TAR}}} p_{l,u} [D_{\text{TAR,min},l} - D_l(\Phi_{0,l})]^2 + \frac{1}{N_{\text{TAR}}} \sum_{l=1}^{N_{\text{TAR}}} p_{l,o} [D_{\text{TAR,max},l} - D_l(\Phi_{0,l})]^2 + \\ + \frac{1}{N_{\text{OAR}}} \sum_{m=1}^{N_{\text{OAR}}} p_{m,o} [D_{\text{OAR,max},m} - D_m(\Phi_{0,m})]^2, \quad (4.2)$$

where  $N_{\text{TAR}}$  stands for the count of targets and  $N_{\text{OAR}}$  for the count of OARs. The prescribed dose is denoted as  $D_{\text{pres}}$ . For each VOI there is also defined a penalty function  $p$ , describing either the overdose level  $p_o$  or underdose level  $p_u$ . The penalty function thus specifies the importance of individual criteria.

Such function can be easily extended into a multi-objective formulation, where each TAR is described by two objectives – first two addends in Equation (4.2) – and each OAR is then addressed by the objective function equal to the last addend in Equation (4.2).

The above formulation is useful because of its convexity (Shao et al., 2008), thus locally optimal solution is also globally optimal (Paganetti, 2012). Another advantage is the simplicity to implement DVH constraints. The main disadvantage is the fact that the weighting factors of individual criteria do not have any clinical meaning and the choice is arbitrary (Shao et al., 2008).

The objective function has been also written in a linear form, hence linear programming can be used (Shepard et al., 1999). The advantage of such approach is the fact that it always generates globally optimal solution and the computation is fast. The LP does however often produce degenerated solutions (i.e. the vertices of objective space), which are clinically not acceptable. Therefore, a multi-objective approach needs to be applied. Note that it is also hard to implement DVH constraints, see (Shao et al., 2008) for details.

### Linear program formulation

Optimization of a proton therapy treatment plan can be formulated as a linear program (LP) minimizing the cumulated sum of all primary fluences, which can be equivalently described as the minimization of the total amount of irradiated protons:

$$\min \sum_{i=1}^n \Phi_{0,i} : \quad \begin{aligned} \sum_{i=1}^n D_{ij}(\Phi_{0,i}) &\leq D_{\text{OAR,max}}, \\ \sum_{i=1}^n D_{ij}(\Phi_{0,i}) &\geq D_{\text{TAR,min}}, \\ \sum_{i=1}^n D_{ij}(\Phi_{0,i}) &\leq D_{\text{TAR,max}}, \\ \forall \Phi_{0,i} &\geq 0, \end{aligned} \quad (4.3)$$

where  $n$  stands for the total count of beams. All conditions are rechecked in each voxel  $j$  independently.

If the LP is feasible, globally optimal solution will be obtained. In most cases the LP is, however, infeasible due to prescribed conflicts in constraints.

The LP is therefore modified into a linear goal program with one-sided free goals, see Section 3.2.4.



For the tumor it is introduced a deviational variable  $\delta_{\text{TAR},\min}$  indicating the level of under-achievement of the minimal required dose in the tumor  $D_{\text{TAR},\min}$  and a deviational variable  $\delta_{\text{TAR},\max}$  indicating the level of over-achievement of the maximal required dose in the tumor  $D_{\text{TAR},\max}$ . Dose in OARs is described by a deviational variable  $\delta_{\text{OAR},\max}$  indicating the level over-achievement of the maximal required dose in OAR  $D_{\text{OAR},\max}$ . The meaning of all the deviational variables is showed in Figure 4.1. The LP is then actually minimizing a penalty function of the cumulated sum of deviational variables. Finally, the LP is written as:

$$\begin{aligned}
 \min \sum \delta : \quad & \sum_{i=1}^n D_{ij}(\Phi_{0,i}) \leq D_{\text{OAR},\max} + \delta_{\text{OAR},\max}, \\
 & \sum_{i=1}^n D_{ij}(\Phi_{0,i}) \geq D_{\text{TAR},\min} - \delta_{\text{TAR},\min}, \\
 & \sum_{i=1}^n D_{ij}(\Phi_{0,i}) \leq D_{\text{TAR},\max} + \delta_{\text{TAR},\max}, \\
 & \forall \Phi_{0,i} \geq 0, \\
 & \forall \delta \geq 0.
 \end{aligned} \tag{4.4}$$

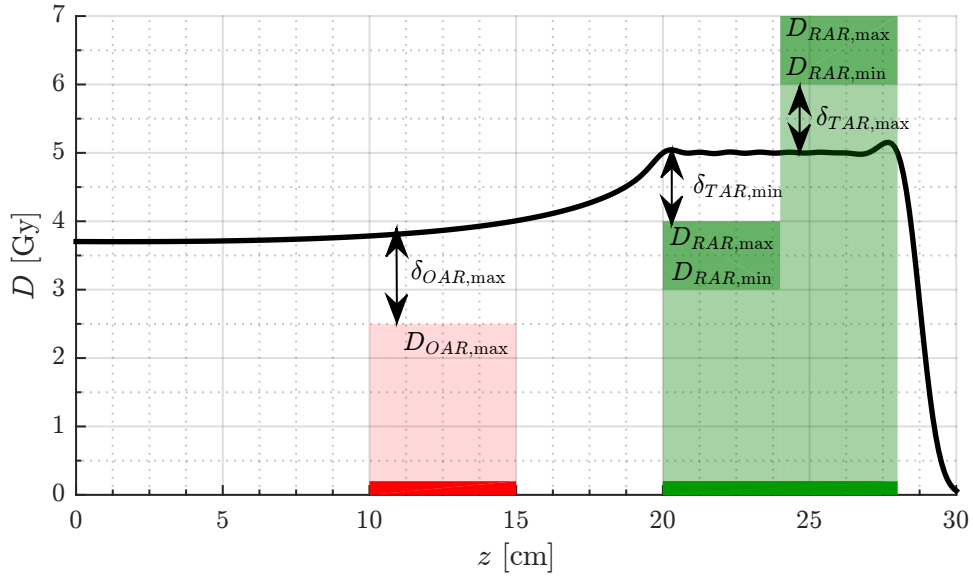


Figure 4.1: Free one-sided goals in optimization of proton therapy treatment plan. Red color symbolizes OAR, green color denotes the tumor.

Although the LP (4.4) is always feasible the resulting solution is mostly degenerated, i.e. one or more deviational variables are equal to zero. It is also preferred to have the ability to choose a custom trade-off between the deviational variables according to DVH.

## Selection of an appropriate solution

To obtain more non-dominated solutions which give the possibility to a decision maker to choose the most appropriate one, all the methods described in Section 3.2 describing MOLP can be used.

Obtained Pareto-optimal solutions can be divided into three groups:

- **Vertex of the polytope.** From the analysis of previously done optimizations it seems that the most of the vertices of the objective space are degenerated solutions of the MOLP.
- **A point on an edge of the polytope.** The solution is degenerated only if the edge is connecting two vertices with the same degenerated deviational variable.
- **A point on a facet of the polytope.** The solution is not degenerated if it is not simultaneously located on the degenerated edge of the polytope.

From the above division it is clear that the most favorable solutions are the ones located on the facets of the polytope. If the solutions are distributed uniformly, the shape of the Pareto surface is sufficiently described. Moreover, the uniformly distributed solutions can offer a sufficient possibility of selection. Therefore, theory described in Section 3.2.6 is used. The precision of such an algorithm is indirectly controlled by the number of uniformly distributed points. Each unique Pareto-optimal solution requires solving just one LP. To compare the inner-approximation with the exact Pareto surface Benson's algorithm has been used, see Section 3.2.5.

## Examples of optimization

This section shows some optimization problem solved with the presented methodologies. Firstly, a LP defined by (4.3) is considered and subsequently, a LP with one-sided free goals is used (see Equation (4.4)). The problem is finally extended to a MOLP and Benson's algorithm and the uniformly-distributed-Pareto-optimal-solutions-method are used.

### Minimization of primary fluences

Both the following two examples of a 1-dimensional optimization are solved as LPs based on Equation (4.3). The LPs are feasible only because of the appropriate constraints.

#### 1D example – one-sided irradiation

The simplest example is a LP with only two design variables  $\Phi_1$  a  $\Phi_2$ , see Figure 4.3. Two Bragg peaks are gradually placed into depths 24 and 28 cm. The OAR is located between 10 and 15 cm, the maximal allowed dose is  $D_{\text{OAR,max}} = 5$  Gy. Tumor is located in the depths between 20 and 28 cm. The maximal dose in tumor is prescribed to be equal to  $D_{\text{TAR,max}} = 10$  Gy, the minimal dose in tumor is  $D_{\text{TAR,min}} = 5$  Gy. All the above conditions are checked within 1 cm precision.

Firstly, individual Bragg curves in significant depths are computed:

Curve	OAR(15)	T(20)	T(21)	T(22)	T(23)	T(24)	T(25)	T(26)	T(27)	T(28)
1	1.089	1.330	1.447	1.623	2.073	2.940	0.798	0.007	0.000	0.000
2	0.978	1.066	1.098	1.139	1.195	1.271	1.383	1.568	1.978	2.657

Table 4.1: 1D example of one-sided irradiation. Dose is computed only in depths, where the constraints are checked.

Subsequently, the inequalities are assembled:

$$\text{OAR: 1) } 1.089\Phi_1 + 0.978\Phi_2 \leq 5$$

$$\text{TAR: 2) } 1.330\Phi_1 + 1.066\Phi_2 \geq 5 \quad 11) 1.330\Phi_1 + 1.066\Phi_2 \leq 10$$

$$3) 1.447\Phi_1 + 1.098\Phi_2 \geq 5 \quad 12) 1.447\Phi_1 + 1.098\Phi_2 \leq 10$$

$$4) 1.623\Phi_1 + 1.139\Phi_2 \geq 5 \quad 13) 1.623\Phi_1 + 1.139\Phi_2 \leq 10$$

$$5) 2.073\Phi_1 + 1.195\Phi_2 \geq 5 \quad 14) 2.073\Phi_1 + 1.195\Phi_2 \leq 10$$

$$6) 2.940\Phi_1 + 1.271\Phi_2 \geq 5 \quad 15) 2.940\Phi_1 + 1.271\Phi_2 \leq 10$$

$$7) 0.798\Phi_1 + 1.383\Phi_2 \geq 5 \quad 16) 0.798\Phi_1 + 1.383\Phi_2 \leq 10$$

$$8) 0.007\Phi_1 + 1.568\Phi_2 \geq 5 \quad 17) 0.007\Phi_1 + 1.568\Phi_2 \leq 10$$

$$9) 0.000\Phi_1 + 1.978\Phi_2 \geq 5 \quad 18) 0.000\Phi_1 + 1.978\Phi_2 \leq 10$$

$$10) 0.000\Phi_1 + 2.657\Phi_2 \geq 5 \quad 19) 0.000\Phi_1 + 2.657\Phi_2 \leq 10$$

$$\text{Non-negativity of fluences: } 1.000\Phi_1 + 0.000\Phi_2 \geq 0$$

$$0.000\Phi_1 + 1.000\Phi_2 \geq 0. \quad (4.5)$$

The objective function is then defined as

$$f = \min (\Phi_1 + \Phi_2). \quad (4.6)$$

Such a simple LP can be solved also graphically. The design space generates a two-dimensional plane  $\mathbb{R}^2$ . The plane is then constrained by the above inequalities.

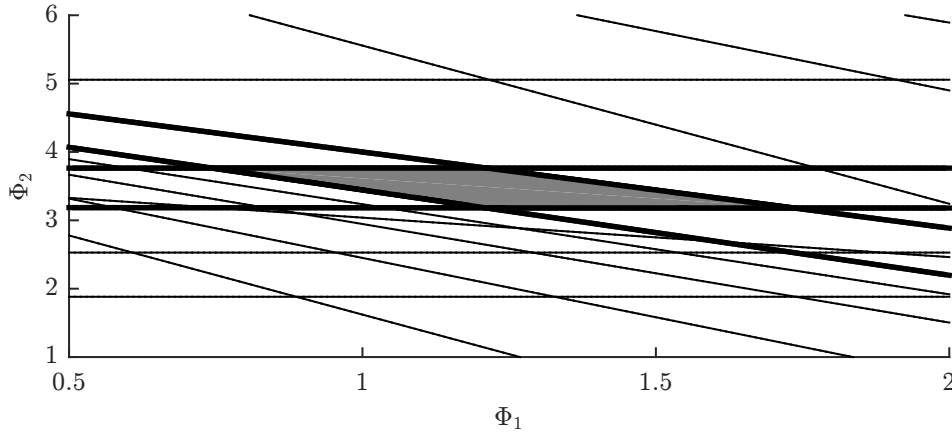


Figure 4.2: Constraints in the 1D proton therapy treatment plan optimization. Gray color represents the set of all feasible solutions.

Figure 4.2 clearly shows that the polytope is constrained by four active constraints (1, 10, 11 and 17). The constraints define four intersections, see Table 4.2.

Bod	$\Phi_1$	$\Phi_2$	$f = \Phi_1 + \Phi_2$
A1	0.744	3.764	4.508
A2	1.210	3.183	4.393
A3	1.212	3.764	4.976
A4	1.735	3.181	4.916

Table 4.2: Vertices of the polytope.

Based on the computed values of the objective function in the specified four points the global minimum is located in the point A2 with the objective 4.393. Subsequently, the globally optimal solution fulfilling all the prescribed constraints is  $\Phi_1$  times multiplication of the Bragg curve with the peak in the distance of 24 cm and a  $\Phi_2$  times multiplication of the Bragg curve with the peak in the distance of 28 cm. The result of the optimization is shown in Figure 4.3. Figure 4.4 then represents DVH<sup>1</sup> of the resulting plan.

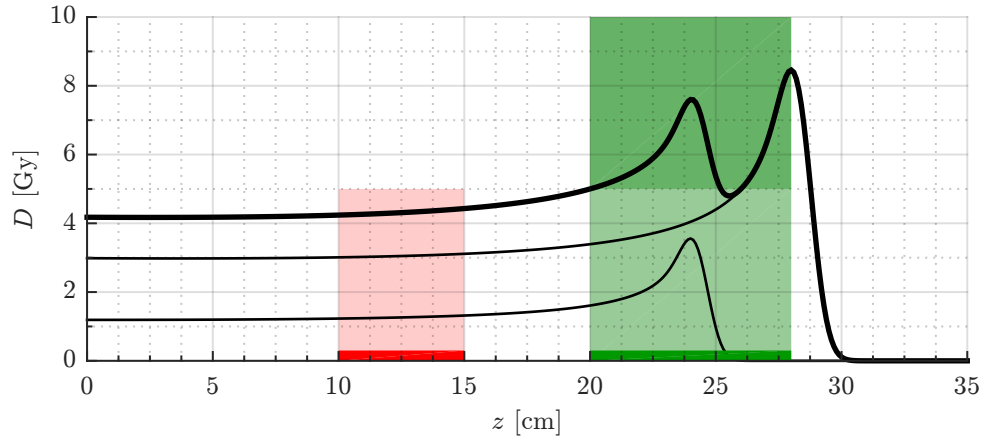


Figure 4.3: Globally optimal solution of a simple 1D treatment plan.

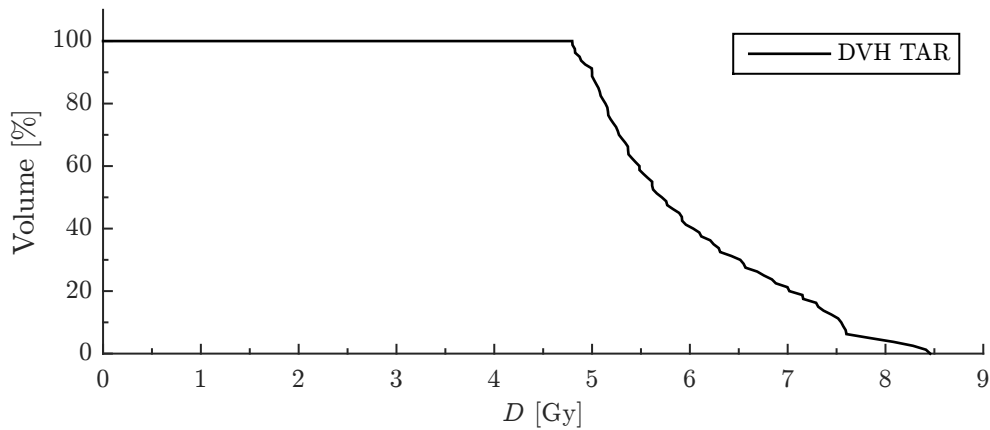


Figure 4.4: Globally optimal solution of a simple 1D treatment plan – DVH of the tumor.

<sup>1</sup>Dose-Volume Histogram indicates the percentage of volume  $V$  that receives at least the dose  $D$ .

### 1D example – double-sided irradiation with the effect of inhomogeneities

In the second example, shown in Figure 4.5, the effect of inhomogeneities is considered. In the depths 10 – 15 cm and 35 – 40 cm bones are located. The tumor is placed between the depths 20 and 30 cm and is irradiated from the both directions, i.e. from depths 0 and 50 cm, respectively. The maximum allowed dose in the tumor is prescribed to be  $D_{\text{TAR,max}} = 10$  Gy, the minimum dose in the tumor is required to be  $D_{\text{TAR,min}} = 5$  Gy. An organ at risk, located between depths 10 and 15 cm, should not receive a dose higher than  $D_{\text{OAR,max}} = 1$  Gy.

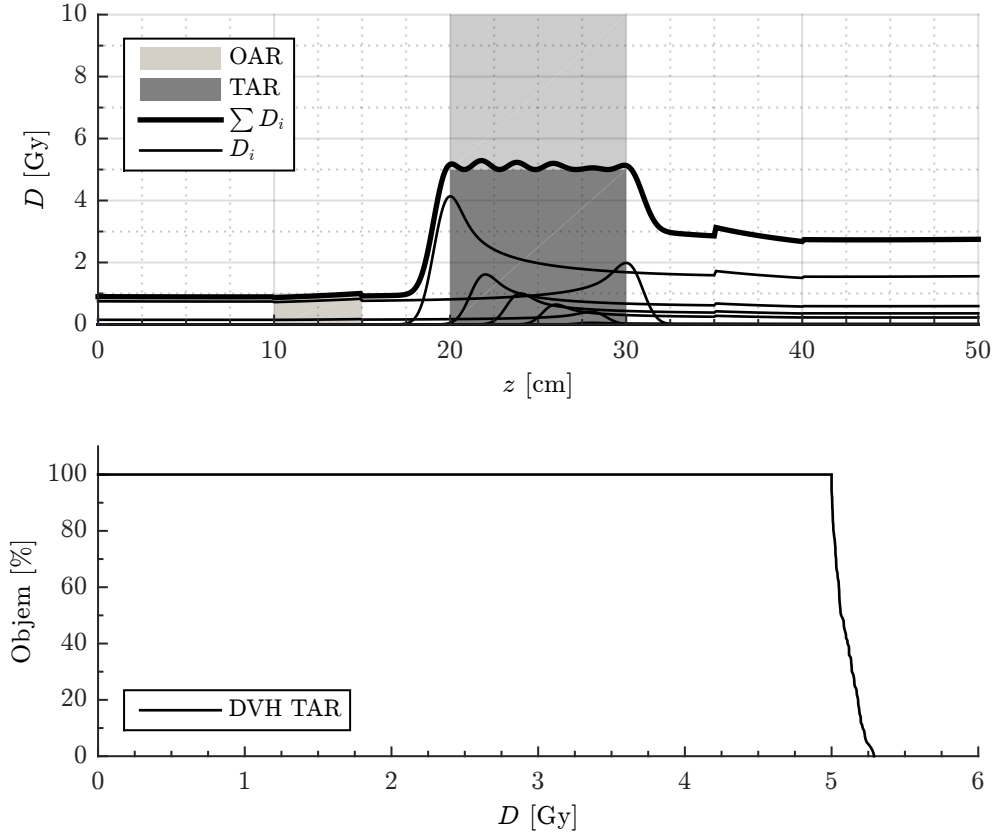


Figure 4.5: Optimal 1D treatment plan accounting the effect of inhomogeneities and double-sided irradiation.

### Linear goal programming

This section presents an example that is not feasible using the previous formulation, see Equation (4.3). The resulting plan does, however, fulfill at least one of the constraint exactly.

### 1D example – double-sided irradiation

Let us consider irradiation from the depths  $z_1 = 0$  cm and  $z_2 = 50$  cm; and the tumor in the depths 20 – 28 cm. The required minimum and maximum doses in the tumor are  $D_{\text{TAR,min}} = 5$  Gy and  $D_{\text{TAR,max}} = 10$  Gy, respectively. Two organs at risk are prescribed in the depths of 10 – 15 cm and 35 – 40 cm, both are assigned the same maximal dose  $D_{\text{OAR,max,1}} = D_{\text{OAR,max,2}} = 1$  Gy.

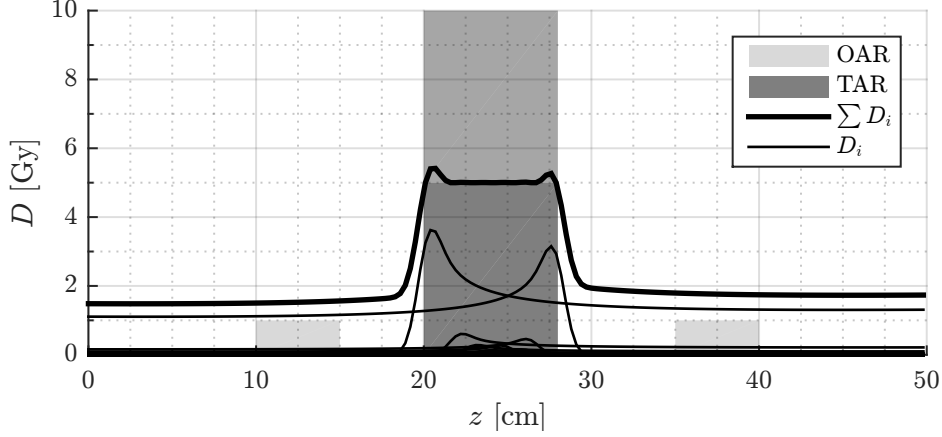


Figure 4.6: Optimal 1D treatment plan optimized using linear goal programming. Double-sided irradiation.

The linear program (4.4) gives the optimum shown in Figure 4.6. From the figure it follows that using the formulation (4.3) we would not obtain any solution, because the problem is infeasible – it is either needed to exceed the maximal required dose in any of the OARs or not to achieve the required dose in the tumor. The optimum obtained by linear goal programming exceeds the maximal dose in both of the OARs, but concurrently fulfills the prescribed minimal dose in the tumor.

### Multi-objective linear goal programming

The multi-objective linear programming enables the decision maker to choose the most appropriate solution among the set of non-dominated (compromise) solutions.

Usually, the decision maker can prescribe a large amount of Pareto-optimal solutions. Therefore, a simple user interface in MATLAB has been implemented enabling the decision maker to graphically select the most appropriate plan based on the deviational variables, i.e. the level of exceeding of individual prescribed doses. The decision maker is thus also given the idea of what will be achieved by using another non-dominated solution, as the deviational variables are given a real physical meaning. Also, the 1D implementation enables us to display multiple optimal solutions concurrently for a comparison.

The user interface does indeed display the DVHs for all the OARs and the tumor(s) to enable the decision maker to evaluate the uniformity of the dose, as this aspect also influences the selection of the most appropriate treatment plan.

In the case of only two or three objective functions it is possible to display either full or approximated version of Pareto surface. If the number of objectives is greater than three then the Pareto surface cannot be effectively displayed and thus all the non-dominated solutions are shown as all the two or three dimensional combinations of the total count of dimensions of the objective space.

### 1D example – double-sided irradiation

Let us consider the last example from the previous section. Also, we will not evaluate the  $D_{\text{TAR,max}}$ , as it does not have any effect on the results (i.e. the associated objective function is always equal to

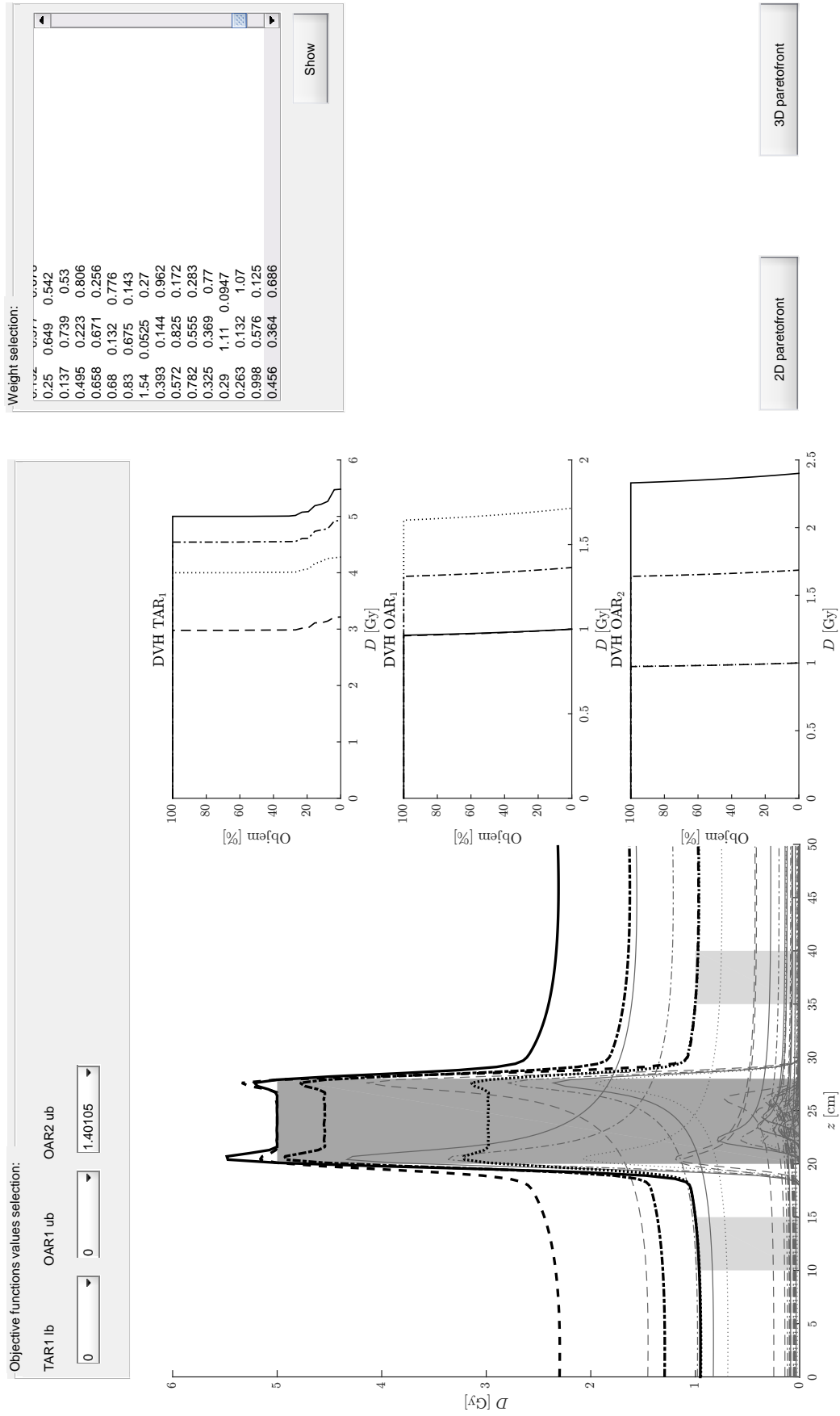


Figure 4.7: Implementation of the user interface for displaying results of 1D multi-objective linear goal program.

zero). Overall, three objective functions are being evaluated:  $\delta_{TAR,min}$ ,  $\delta_{OAR,max,1}$  and  $\delta_{OAR,max,2}$ .

The result of the created program is shown in Figure 4.7, actually, four optimal non-dominated solutions are displayed concurrently: the solid line denotes a solution with the objectives  $\delta_{TAR,min}$  and  $\delta_{OAR,max,1}$  equal to zero. The dotted line denotes a solution with null objectives  $\delta_{OAR,max,1}$  and  $\delta_{OAR,max,2}$ . The dashed line represents a solution when both the  $\delta_{TAR,min}$  and  $\delta_{OAR,max,2}$  objectives are equal to zero. Therefore, the already described solutions apparently serve as the extreme solutions defining the boundary of the Pareto surface. As the last non-dominated solution we have chosen a point that is located on one of the facets of the Pareto surface, i.e. none of the objectives is equal to zero. This solution is displayed by a dash-dot line.

Secondly, the program enables us to render the Pareto surface, see Figure 4.8. From the figure it implies all the vertices of the Pareto surface (177 black points) are located on the frontier of the objective space; and the edges of the Pareto surface lying in planes  $\delta_{OAR,max,1} = 0$  and  $\delta_{OAR,max,2} = 0$  are straight, forming thus lines. The intersection of the Pareto surface and the plane  $\delta_{TAR,min} = 0$  is, on the contrary, not straight.

The red points in Figure 4.8 denote non-dominated solutions uniformly distributed on the Pareto surface generated by the modified `distmesh` algorithm. It should be noted that due to the clarity of the resulting image we have not displayed points located on the edge of the Pareto surface.

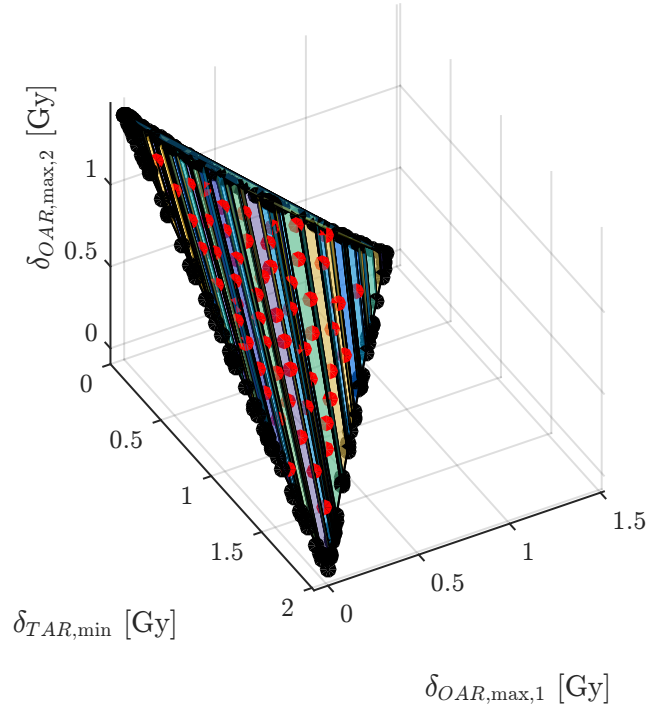


Figure 4.8: Implementation of the user interface for displaying the results of linear goal program – Pareto surface.

### 3D example – one-sided irradiation

In the 3D case the tumor is irradiated from a plane defined by the plane equation  $ax + by + cz + d = 0$  in a direction specified by a directional vector  $\vec{u} = (x, y, z)$ . The geometry of the environment and of



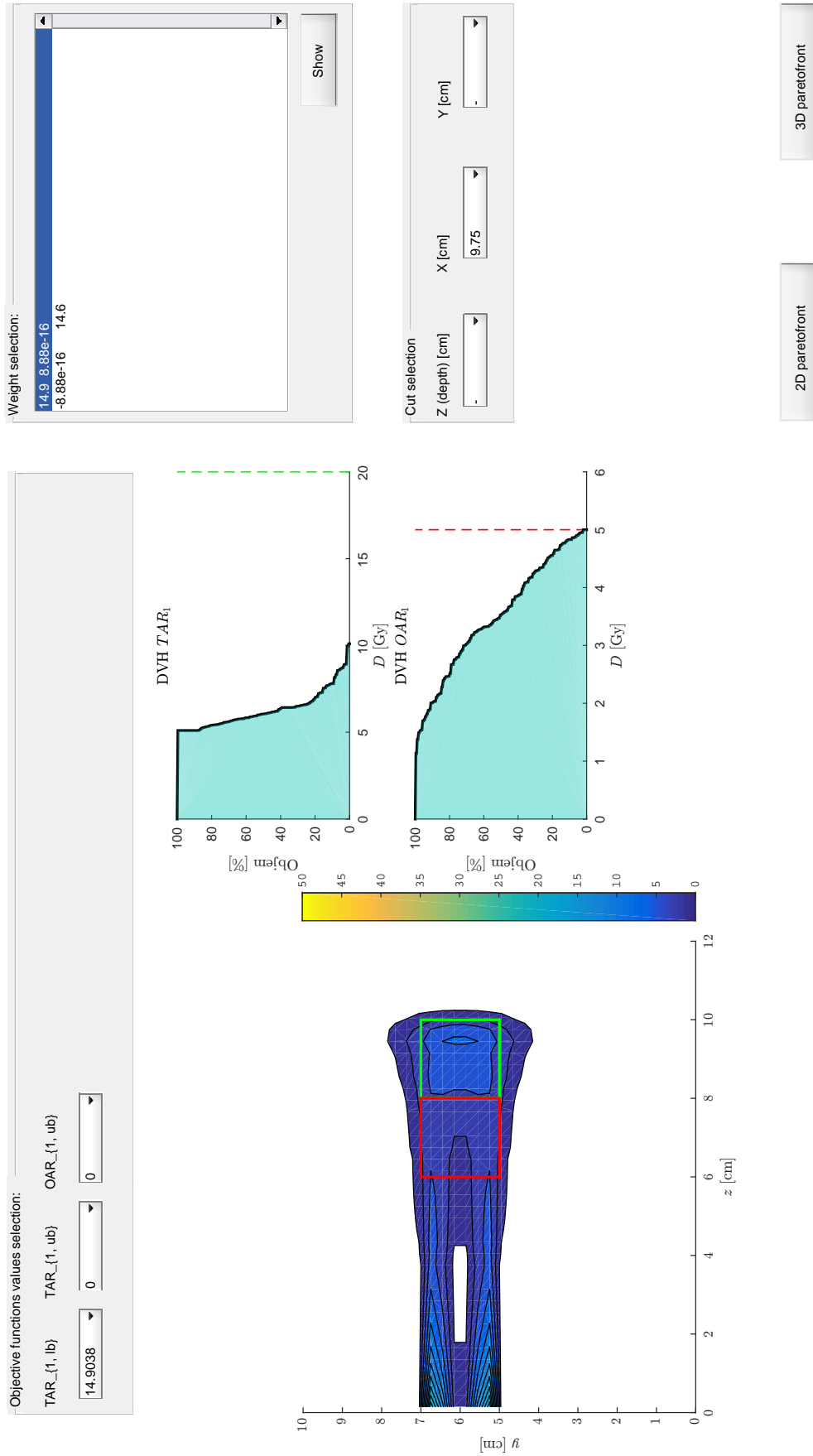


Figure 4.9: Implementation of the user interface for displaying results of the multi-objective linear goal program for the 3D treatment plan. The cut at plane  $x = 9.75$  cm is displayed. The red color denotes OAR, the green color represents the tumor.

anatomically important structures (TAR and OAR) is described by linear inequalities. Although the structures are generally non-convex, they can be still assembled from multiple convex parts.

We will now evaluate a simple treatment plan defined by limit values  $D_{\text{TAR},\min} = 20$  Gy,  $D_{\text{TAR},\max} = 40$  Gy and  $D_{\text{OAR},\max} = 5$  Gy and by geometry of the surroundings of the tumor:

$$\begin{aligned}
 \text{TAR :} \quad & z \geq 8 \wedge z \leq 10 \\
 & x \geq 8 \wedge x \leq 10 \\
 & y \geq 5 \wedge y \leq 7 \\
 \text{OAR :} \quad & z \geq 6 \wedge z \leq 8 \\
 & x \geq 8 \wedge x \leq 10 \\
 & y \geq 5 \wedge y \leq 7 \\
 \text{Cyclotron :} \quad & \vec{u} = (0; 0; 1) \\
 & x + y + 0z - 8 = 0.
 \end{aligned} \tag{4.7}$$

The optimized treatment plan is shown in Figure 4.9. Because the objective  $\delta_{\text{TAR},\max}$  is degenerated (null), again, the number of objectives is reduced to two –  $\delta_{\text{TAR},\min}$  and  $\delta_{\text{OAR},\max}$ . The shape of the Pareto surface is shown in Figure 4.10.

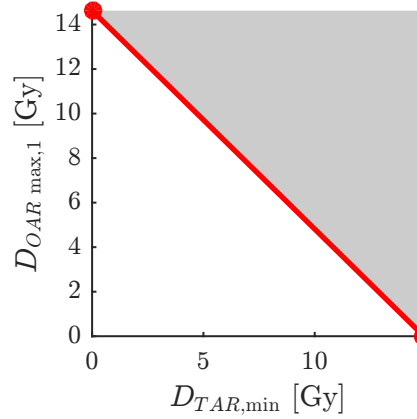


Figure 4.10: Implementation of the user interface for displaying results of the multi-objective linear goal program for 3D treatment plan – 2D Pareto surface.

### 3D example – double-sided irradiation

The last example presents an optimization of a 3D treatment plan comprising the irradiation from multiple, here two, directions. The location of the tumor and of the OAR is the same as in the previous section, the only difference is the location of the cyclotron:

$$\begin{aligned}
\text{Cyclotron : } \quad \vec{u}_1 &= (0; -0.2; 0.7) \\
\vec{u}_2 &= (0; 0.3; 0.7) \\
0x + 1y + 4z - 10 &= 0.
\end{aligned} \tag{4.8}$$

We evaluate the objective functions  $\delta_{\text{TAR},\min}$  and  $\delta_{\text{OAR},\max}$  and the result is similar to the previous example – the Pareto surface can be described as a linear combination of two extreme solutions, see Figure 4.11 and Figure 4.12. The cut is taken through  $x = 9.75$  cm.

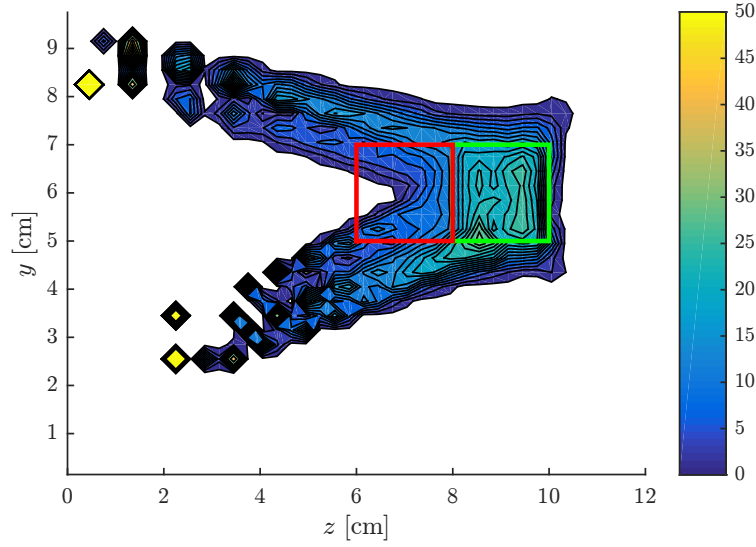


Figure 4.11: 3D treatment plan accounting double-sided irradiation. The non-dominated solution shown in the figure conserves the required dose  $D_{\text{TAR},\min}$ .

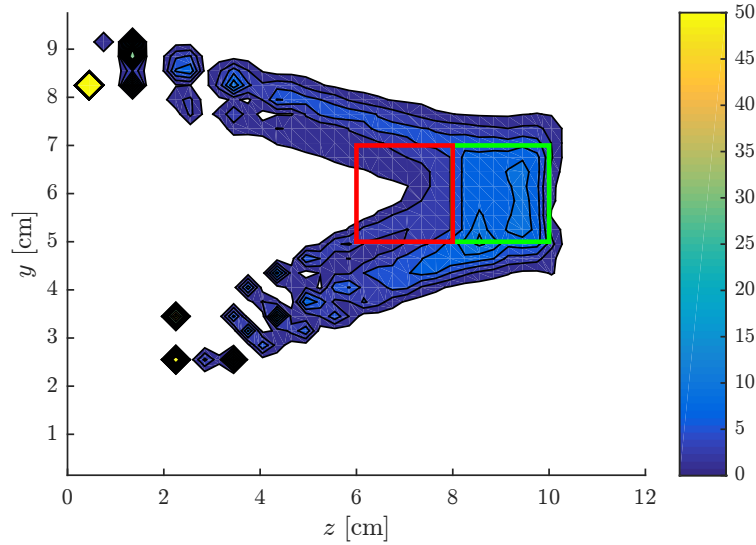


Figure 4.12: 3D treatment plan accounting double-sided irradiation. The non-dominated solution shown in the figure conserves the required dose  $D_{\text{OAR},\max}$ .

## Time demands of the optimization using Benson's algorithm

All the listed examples of optimization have been evaluated on a common computer<sup>2</sup>. The results in Table 4.3 are valid only for the non-parallel and parallel version of Benson's algorithm. The times of uniform distribution of solutions on the Pareto surface have not been exactly measured yet, but the implementation reaches significant speedup compared to the Benson's algorithm.

The results in Table 4.3 implies that the time, respectively computational demands, of Benson's algorithm are dependent on the count of inequalities  $N_{\text{constr.}}$  – i.e. the sizes of VOIs (the tumor size  $V_{\text{TAR}}$  and the OARs size  $V_{\text{OAR}}$ ) and on the voxel grid fineness.

The negative effect on the speed of Benson's algorithm also have the growing number of objective functions  $N_{f(x)}$  and the number of design variables  $N_x$ , i.e. irradiation from multiple directions. Of the most important influence is, however, the segmentation of the Pareto surface: the higher the total count of vertices the greater the count of linear programs which are needed to be solved. Unluckily, the total number of vertices is not known in advance.

$V_{\text{tot}}$	$V_{\text{TAR}}$	$V_{\text{OAR}}$	$N_{\text{constr.}}$	$N_x$	$N_{f(x)}$	$N_{\text{vert}}$	$t_{\text{gen}} [\text{s}]$	$t_{\text{opt,non}} [\text{s}]$	$t_{\text{opt,par}} [\text{s}]^3$
43.560	216	252	686	218	2	2	2.613	0.655	16.632
43.560	216	588	1.239	435	3	21	3.965	6.074	16.856
66.424	392	448	2.019	787	3	57	8.143	51.993	47.237
25.872	180	330	873	363	3	455	2.775	118.950	90.645
43.560	216	588	1.239	435	3	525	3.874	165.352	128.420
43.560	216	588	1.239	435	3	649	3.894	209.533	144.563
76.800	512	512	2.563	1.027	3	201	11.337	285.529	222.354
88.200	648	576	3.176	1.299	3	182	16.102	457.189	334.597

Table 4.3: Time demands of the treatment plan optimization using Benson's algorithm.  $V_{\text{tot}}$  denotes the total count of voxels,  $V_{\text{TAR}}$  the number of voxels in the tumor(s),  $V_{\text{OAR}}$  the number of voxels on OAR(s), respectively.  $N_{\text{constr.}}$  represents the total count of constraints of the LP,  $N_x$  the number of design variables,  $N_{f(x)}$  the number of objective functions and  $N_{\text{vert}}$  the total count of vertices forming the full Pareto surface.  $t_{\text{gen}}$  denotes the time needed to calculate the doses,  $t_{\text{opt,non}}$  represents the time needed for the non-parallel version of Benson's algorithm to obtain full Pareto-surface. The time needed for the parallel version of Benson's algorithm is denoted by  $t_{\text{opt,par}}$ .

Note that based on (Shao et al., 2008) it is possible to implement an approximate version of Benson's algorithm, such that the time and computational demands are significantly lowered.

<sup>2</sup>We have used MATLAB R2014b on a laptop Acer Aspire V15 with processor Intel Core i5-4210H 2.90 GHz and RAM 8 GB DDR3L SDRAM. Ubuntu 14.04 64bit has been used as the OS.

<sup>3</sup>Opening of the parallel pool in MATLAB tooks 11.5 s. Two computational cores have been used.

## Chapter 5

# Conclusion

In this thesis it has been described an implementation of a simplified model of the beam propagation through matter. An analytical approximation of the Bragg curve has been implemented incorporating the influence of inhomogeneities. The multiple scattering theory has been included by the implementation of Highland's approximation. Based on the compared values sufficiently accurate results have been achieved.

Subsequently, the key part of this thesis – optimization of the proton therapy treatment plan – has been introduced. Firstly, we have adopted a linear program minimizing the total count of irradiated protons (resp. the primary fluences). The common weakness of the approach has proved to be non-feasibility of the program duo to conflicting constraints.

Hence, the linear program has been reformulated into a linear program with free one-sided goals, ensuring thus the feasibility of the optimization and presenting certain freedom in the prescribed constraints. The optimal solution is, however, usually degenerate and is therefore not appropriate for practical use.

The optimization problem has been finally modified into multiple-objective linear programming with free one-sided goals, enabling thus the decision maker to choose the most appropriate solution within the whole (infinitesimal) Pareto surface. The whole and exact Pareto surface is obtained using either parallel or non-parallel version of Benson's algorithm.

Because the time demands of Benson's algorithm cannot be guaranteed in advance a new approach creating uniformly distributed points on the Pareto surface has been developed. The approach is based on the modified algorithm `distmesh` and ensures the possibility to approximate the whole Pareto surface. Also, the approach is ideally parallelizable, because the individual uniformly distributed points are mutually independent.

# Bibliography

- Zdravotnická statistika - Zemřelí 2012* [online]. Ústav zdravotnických informací a statistiky České republiky, 2013. [cit. 2. 4. 2015]. Available at: [www.uzis.cz/system/files/demozem2012.pdf](http://www.uzis.cz/system/files/demozem2012.pdf).
- BENSON, H. P. An outer approximation algorithm for generating all efficient extreme points in the outcome set of a multiple objective linear programming problem. *Journal of Global Optimization*. 1998, 13, 1, s. 1–24.
- BERGER, M. J. et al. Stopping powers and ranges for protons and alpha particles. *ICRU Report*. 1993, 49.
- BETHE, H. Moliere's theory of multiple scattering. *Physical Review*. 1953, 89, 6, s. 1256.
- BOKRANTZ, R. Multicriteria optimization for managing tradeoffs in radiation therapy treatment planning. 2013.
- BORTFELD, T. An analytical approximation of the Bragg curve for therapeutic proton beams. *Medical physics*. 1997, 24, 12, s. 2024–2033.
- CHEN, P.-C. – HANSEN, P. – JAUMARD, B. On-line and off-line vertex enumeration by adjacency lists. *Operations Research Letters*. 1991, 10, 7, s. 403–409.
- CODERRE, J. *Principles of Radiation Interactions* [online]. 2004. [cit. 8. 4. 2014]. Available at: [http://ocw.mit.edu/courses/nuclear-engineering/22-55j-principles-of-radiation-interactions-fall-2004/lecture-notes/energy\\_depos\\_hcp.pdf](http://ocw.mit.edu/courses/nuclear-engineering/22-55j-principles-of-radiation-interactions-fall-2004/lecture-notes/energy_depos_hcp.pdf).
- VERA, P. – ABRIL, I. – GARCIA-MOLINA, R. Water equivalent properties of materials commonly used in proton dosimetry. *Applied Radiation and Isotopes*. 2014, 83, s. 122–127.
- DEMEL, J. *Operační výzkum* [online]. 2011. [cit. 8. 4. 2014]. Available at: <http://kix.fsv.cvut.cz/~demel/ped/ov/ov.pdf>.
- DEVROYE, L. Sample-based non-uniform random variate generation. In *Proceedings of the 18th conference on Winter simulation*, s. 260–265. ACM, 1986.
- EVANS, N. *PHYS3016: lecture 28th February 2008* [online]. 2008. [cit. 8. 4. 2014]. Available at: <http://www.southampton.ac.uk/~evans/PHYS3017/Rel.pdf>.

- FIGUEIRA, J. – GRECO, S. – EHRGOTT, M. *Multiple criteria decision analysis: state of the art surveys*. 78. Springer Science & Business Media, 2005.
- GALE, D. – KUHN, H. W. – TUCKER, A. W. Linear programming and the theory of games. *Activity analysis of production and allocation*. 1951, 13, s. 317–335.
- GOTTSCHALK, B. et al. Multiple Coulomb scattering of 160 MeV protons. *Nuclear Instruments and Methods in Physics Research Section B: Beam Interactions with Materials and Atoms*. 1993, 74, 4, s. 467–490.
- GOTTSCHALK, B. On the scattering power of radiotherapy protons. *Medical physics*. 2009, 37, 1, s. 352–367.
- GUPTA, M. Calculation of radiation length in materials. Technical report, 2010.
- HIGHLAND, V. L. Some practical remarks on multiple scattering. *Nuclear Instruments and Methods*. 1975, 129, 2, s. 497–499.
- HONG, L. et al. A pencil beam algorithm for proton dose calculations. *Physics in medicine and biology*. 1996, 41, 8, s. 1305.
- HUSSEIN, E. *Handbook on Radiation Probing, Gauging, Imaging and Analysis: Volume II Applications and Design*. Basics and techniques. Springer, 2003. ISBN 9781402012952.
- HYNKOVÁ, L. – DOLEŽELOVÁ, H. – ŠLAMPA, P. *Radioterapie - učební texty pro studenty 5. roč. LF MU Brno* [online]. [cit. 2.4.2015]. Available at: <https://www.mou.cz/radioterapie-ucebni-texty-pro-studenty-5-roc-lf-mu-brno/f16>.
- JABLONSKÝ, J. *Vícekritériální a cílové programování* [online]. [cit. 8.4.2014]. Available at: <http://nb.vse.cz/~JABLON/doc/vkr.pdf>.
- JABLONSKÝ, J. *Operační výzkum: kvantitativní modely pro ekonomické rozhodování*. Professional Publishing, 2002.
- JANNI, J. F. Proton Range-Energy Tables, 1 keV-10 GeV, Energy Loss, Range, Path Length, Time-of-Flight, Straggling, Multiple Scattering, and Nuclear Interaction Probability. Part II. For 92 Elements. *Atomic Data and Nuclear Data Tables*. 1982, 27, s. 341.
- JONES, D. – TAMIZ, M. *Practical goal programming*. Springer, 2010. ISBN 1441957715.
- KLEDER, M. *CON2VERT - constraints to vertices - File Exchange - MATLAB Central* [online]. 2005. [cit. 1.4.2015]. Available at: <http://www.mathworks.com/matlabcentral/fileexchange/7894-con2vert-constraints-to-vertices>.
- KRESS, R. *Numerical Analysis*. Graduate Texts in Mathematics. Springer New York, 1998. Available at: <http://books.google.cz/books?id=R6182rh0tKEC>. ISBN 9780387984087.

- LANG, S. – RIESTERER, O. *Modern Techniques in Radiation Oncology* [online]. 2013. [cit. 8.4.2014]. Available at: [http://www.sps.ch/artikel/progresses/modern\\_techniques\\_in\\_radiation\\_oncology\\_36](http://www.sps.ch/artikel/progresses/modern_techniques_in_radiation_oncology_36).
- LÖHNE, A. *Vector optimization with infimum and supremum*. Springer Science & Business Media, 2011.
- LUPTÁCIK, M. *Mathematical Optimization and Economic Analysis (Springer Optimization and Its Applications)*. Springer, 2009. ISBN 0387895515.
- MOLIÈRE, v. G. Theorie der Streuung schneller geladener Teilchen I. Einzelstreuung am abgeschirmten Coulomb-Feld. *Zeitschrift Naturforschung Teil A*. 1947, 2, s. 133.
- MOLIÈRE, v. G. Theorie der Streuung schneller geladener Teilchen II. Mehrfach-und Vielfachstreuung. *Zeitschrift Naturforschung Teil A*. 1948, 3, s. 78.
- MYŠÁKOVÁ, E. Optimalizace uniformity počítačových návrhů pro omezené návrhové prostory. Master's thesis, Katedra mechaniky, Fakulta stavební, České vysoké učení technické v Praze, 2013.
- OLIVE, K. – GROUP, P. D. – OTHERS. Review of particle physics. *Chinese Physics C*. 2014, 38, 9, s. 090001.
- PAGANETTI, H. *Proton Therapy Physics*. Series in Medical Physics and Biomedical Engineering. CRC Press/Taylor & Francis, 2012. ISBN 9781439836446.
- PERSSON, P.-O. – STRANG, G. A simple mesh generator in MATLAB. *SIAM review*. 2004, 46, 2, s. 329–345.
- PETIT, S. – SECO, J. – KOOY, H. Increasing maximum tumor dose to manage range uncertainties in IMPT treatment planning. *Physics in medicine and biology*. 2013, 58, 20, s. 7329.
- PFLUGFELDER, D. Risk-adapted optimization in intensity modulated proton therapy (IMPT). 2008.
- PFLUGFELDER, D. et al. A comparison of three optimization algorithms for intensity modulated radiation therapy. *Zeitschrift für Medizinische Physik*. 2008, 18, 2, s. 111–119.
- SCHLEGEL, W. – BORTFELD, T. – GROSU, A. *New Technologies in Radiation Oncology*. Medical Radiology / Radiation Oncology. Springer, 2006. ISBN 9783540003212.
- SHAO, L. – OTHERS. *Multiple objective linear programming in radiotherapy treatment planning*. PhD thesis, ResearchSpace@ Auckland, 2008.
- SHEPARD, D. M. et al. Optimizing the delivery of radiation therapy to cancer patients. *Siam Review*. 1999, 41, 4, s. 721–744.
- TAHERI-KADKHODA, Z. et al. Intensity-modulated radiotherapy of nasopharyngeal carcinoma: a comparative treatment planning study of photons and protons. *Radiat Oncol*. 2008, 3, 4.
- TYBUREC, M. Rozšíření programu distmesh pro vícedimenzionální problémy. *Sborník abstraktů Studentské konference a Rektorysovy soutěže*. 2014a.



- TYBUREC, M. Optimalizace léčebného plánu protonové terapie. *XV. ročník Mezinárodní konference SVOČ: sborník studentských prací 2014*. 2014b.
- WCRF.ORG. *Data for cancer frequency by country — World Cancer Research Fund International* [online]. 2015. [cit. 2. 4. 2015]. Available at: <http://www.wcrf.org/int/cancer-facts-figures/data-cancer-frequency-country>.
- WEISSTEIN, E. W. *Parabolic cylinder function* [online]. 2005. [cit. 8. 4. 2014]. Available at: <http://mathworld.wolfram.com/ParabolicCylinderFunction.html>.
- ZHANG, R. – NEWHAUSER, W. D. Calculation of water equivalent thickness of materials of arbitrary density, elemental composition and thickness in proton beam irradiation. *Physics in medicine and biology*. 2009, 54, 6, s. 1383.
- ZHANG, R. et al. Water equivalent thickness values of materials used in beams of protons, helium, carbon and iron ions. *Physics in medicine and biology*. 2010, 55, 9, s. 2481.

## Appendix A

# Modified algorithm `distmesh`

The algorithm `distmesh` (Persson, Strang, 2004) has been written in the software MATLAB as a simple tool aimed for mesh generation. The fundamental principle of the algorithm is based on dynamic relaxation. The usage of the algorithm in the context of this thesis is focused, however on *Design of Experiments* (DoEs). Compared to faster algorithms, such as `clustering`, the considered algorithm excels specifically in the quality of the resulting design, see (Myšáková, 2013) for reference.

Initially, the algorithm accepts a set of design points  $P$  located in the design space  $N$ . The shape of the design space is stated by the distance function  $d(x_1, \dots, x_n)$  defined as

$$\begin{aligned} d(x_1, \dots, x_n) &\leq 0 \text{ for } x \in N \\ d(x_1, \dots, x_n) &> 0 \text{ for } x \notin N, \end{aligned} \tag{A.1}$$

where  $n$  denotes the number of dimensions of the design space.

The initial points  $P$  are then triangulated by Delaunay's triangulation, crating thus connections between individual points. Similarly to truss structures the individual points then represents nodes and the connections bars of the truss. Also, there is likewise defined a relation between applied forces and displacements.

Let us denote the optimal length of bars by  $L_0$  and the actual length of bars by  $L$ . Based on their difference we will define applied forces  $F$ :

$$F = L_0 - L. \tag{A.2}$$

The applied forces in all nodes are then decomposed into all directions (dimensions). Subsequently, we can introduce displacements  $\Delta P$  dependent on the selected time step  $\Delta t$ . The location of the nodes after the time step is computed as

$$P = P + \Delta P = P + \Delta t F. \tag{A.3}$$

If any of the points move out of the prescribed design space  $N$  an external loading is applied, such that the point moves back into the design space. The direction of the external loading is in the direction of the gradient of distance function.

In the case that all of the points move less than the prescribed tolerance, the final solution is obtained. Otherwise, the points serve as the re-input for the Delaunay's triangulation. The algorithm can also terminate in the case of exceeding of the maximum count of iterations.

In the paper (Tyburec, 2014a) we have modified the algorithm in such a way, that the most time demanding part, Delaunay's triangulation, is replaced by the connection of  $s$  nearest neighbor points, i.e. each point creates at least  $s$  connections. The neighbor connections have been found using MATLAB's internal function `knnsearch`.

An example of the solved two-dimensional problem is shown in Figure A.1.

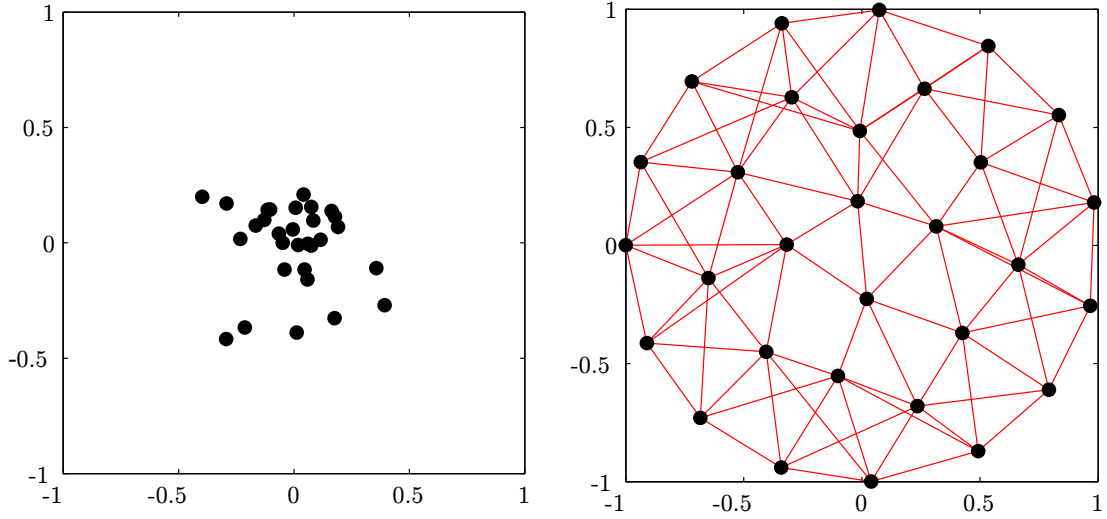


Figure A.1: Example of 2D problem solved by modified algorithm *distmesh*. The left figure shows the initial 30 randomly generated points  $P$ . For each point 5 nearest neighbors have been considered. The right figure shows the result after 100 iterations. The design space is prescribed to be a circle with a radius equal to 1.

Based on the measured values it has been determined that the modification significantly speeded the algorithm up and consequently enabled us to use the algorithm for larger number of dimensions compared to the original version. The quality of the results have proved to be comparable.

## Appendix B

# Numerical solution of definite integrals

There exist situations, where it is not possible to formulate a result of a definite integral by symbolic notation. It is then needed to compute the solution of such definite integrals numerically. The only required inputs are functional values of the specified function in dedicated points. Then, based on the specified accuracy, the points are connected by a polynomial function, for which the integral can be formulated easily.

Generally, the specified interval is split into multiple subintervals, according to needed numerical accuracy. In each subinterval  $n$  functional values are computed, where  $n$  denotes the polynomial lemniscate. Commonly used polynomials are of lemniscate lower than 4 (Kress, 1998).

$$\int_a^b f(x)dx \approx \frac{b-a}{n} [c_1 f(x_0) + \dots + c_n f(x_n)]. \quad (\text{B.1})$$

n	Name of rule	Coefficients $c$				
0	Midpoint	1				
1	Trapezoid	$\frac{1}{2}$		$\frac{1}{2}$		
2	Simpson's	$\frac{1}{3}$	$\frac{4}{3}$	$\frac{1}{3}$		
3	Newton's $^3/8$	$\frac{3}{8}$	$\frac{9}{8}$	$\frac{9}{8}$	$\frac{3}{8}$	
4	Milneo's	$\frac{14}{45}$	$\frac{64}{45}$	$\frac{24}{45}$	$\frac{64}{45}$	$\frac{14}{45}$